EXTREME TEMPERATURE OCCURRENCES OVER EAST ASIA

A THESIS SUBMITTED TO THE GRADUATE DIVISION OF THE UNIVERSITY OF HAWAII MANOA IN PARTIAL FULFILLMENT OF THE REQUIREMENTS FOR THE DEGREE OF

MASTER OF SCIENCE

IN

METEOROLOGY

DECEMBER 2011

By

Hiroyuki Ito

Thesis Committee:

Shang-Ping Xie, Chairperson

Kevin P. Hamilton

Yi-Leng Chen

ACKNOWLEDGMENTS

I am to be grateful to my advisor Dr. Shang-Ping Xie for his time and dedication towards my research progress and the completion of my thesis. I would also like to thank my committee members Dr. Kevin P. Hamilton and Dr. Yi-Leng Chen for their suggestions that led to improvements in my thesis.

I would like to thank Nat Johnson of the International Pacific Research Center, the co-advisor of my thesis, for his advice on many technical issues and support toward accomplishing my goals.

This study is supported by Japan Agency for Marine-Earth Science and Technology (JAMSTEC), National Oceanic and Atmospheric Administration (NOAA), and National Science Foundation (NSF).

ABSTRACT

Extreme daily surface air temperature (SAT; 10^{th} and 90^{th} percentiles) occurrences over East Asia are investigated in relation to seasonal mean and subseasonal variations of SAT as well as to modes of large-scale climate variability, including the Arctic Oscillation, East Asia Winter Monsoon, El Nino Southern Oscillation, and Pacific-Japan teleconnection. Linear regression analysis reveals that seasonal mean shifts of the distribution have a predominant impact on the number of cold and warm extreme days on interannual time scales. Advection of the climatological SAT gradient by anomalous winds is a major mechanism for the winter seasonal mean variability. In contrast, the summer seasonal mean variability is explained by diabatic heating due to downward solar radiation, which is associated with anomalous mid-troposphere circulation that controls total cloud amounts. Advection of SAT by anomalous surface winds is also confirmed for causing anomalies of summer seasonal mean SAT. Regions where extreme occurrences are influenced by the subseasonal SAT variability are extracted by taking the asymmetric component of regression coefficients between the number of cold and warm extreme days. In winter, the subseasonal SAT variability is related to meridional heat transport by transient eddies. In summer, by contrast, it seems to be influenced by both storm activity and precipitation. The frequency distributions of daily SAT anomalies, in relation to modes of climate variability, are generally robust between the reanalysis and station data, in terms of the mean shifts and changes in the standard deviation.

TABLE OF CONTENTS

LIST OF TABLES

LIST OF FIGURES

CHAPTER 1

INTRODUCTION

1.1 Background

Extreme weather occurrences such as heat waves, cold surges, windstorms, extreme precipitation, and drought are of great concern in human society because of their life-threatening impacts and economical damages to industries. According to Munich Re (2002), the number of extreme climate-related events throughout the world has increased last few decades and the associated economical losses have also increased due to the higher population density in hazardous areas than in the past decades. Thus, study of climatic extremes requires a focus in research communities in order to project the possible shifts in frequency and intensity of extreme climatic events such as storms, floods, and heat waves following climate change due to the increase in atmospheric greenhouse gases (Beniston and Stephenson, 2004).

1.2 Previous studies regarding extreme events

It was quite recent that the theory of Generalized Extreme Value (GEV) in the context of climate change was applied, focusing on block maxima (e.g., the single highest daily precipitation amount over an entire year or the highest temperature over a season), although statistical theory of extreme value has been developed extensively under the assumption of stationary (Cooley 2009, Katz 2010). In recent years, many researchers have examined changes in shape of the distribution on extreme occurrences since it was pointed out that the frequency of extreme events might be more sensitive to changes in the standard deviation than that in the mean of distributions (Katz and Brown, 1992). It is argued that changes in extremes can be more reliably derived indirectly from changes in

the overall probability distribution of a climate variable than through direct statistical modeling of extremes (Ballester, 2010). Moreover, it is suggested that not only the frequency, but also the variations in intensity of extremes, as well as the physical appeal of a consistent shift in the entire distribution need to be taken account in extreme studies (Katz 2010).

Extreme studies have been discussed as being coupled with large-scale circulations such as El Nino Southern Oscillation (ENSO; Kiladis and Diaz, 1987, Deser and Wallace 1987), the North Atlantic Oscillation (NAO, Hurrel et al 2003, Wettstein and Mearns 2002), and the Arctic Oscillation (AO, Thompson and Wallace 1999) that is closely related to NAO. For example, it is found that there are large changes in the frequency of 10^{th} percentile temperature and 90^{th} percentile precipitation events over Europe in winter, associated with changes in NAO (Scaife et al. 2007). In the continental Unite States, changes in the number of daily temperature extremes in winter have been considerably related to interannual variability related to ENSO and AO and these changes are consistent with a change in the daily mean Surface Air Temperature (SAT) variability (Higgins et al. 2001). On the worldwide scale, Kenyon and Hegerl (2007) showed that summer and winter temperature extremes are substantially affected by large-scale circulation patterns such as ENSO, NAO, and the Pacific Decadal Oscillation (PDO, Mantua and Hare 2002, Mantua et al 1997). Moreover, they showed distinct regional patterns of response to modes of climate variability that influence the shape of the daily temperature distribution beyond a simple shift, and thereby influencing cold and warm extremes. Gong and Ho (2003) investigated the intra-seasonal variance of SAT over East Asia in winter. The intra-seasonal SAT variance generally has decreased on long term

trend, resulting in less variation in SAT. They also showed that the intra-seasonal variance of both the Siberian High and AO has a significant impact on the temperature variation, although only the seasonal mean AO amplitude influences the temperature variability over East Asia.

1.3 East Asia Surface Air Temperature (SAT) Variability

a. Wintertime Interannual Variability

The interannual variability of SAT over East Asia has been extensively investigated over the last few decades. The SAT variability over East Asia is strongly associated with the Asian Monsoon, one of the largest circulation systems on earth driven by the Siberia-Mongolia High (Chang et al. 2006; Webster et al. 2006). This results from the differential heating between the world's largest continent (i.e. Eurasia) and the Indo-Pacific Ocean, the swirl induced by the rotation of the earth, and moist processes.

In winter, the fluctuation of the East Asian Winter Monsoon (EAWM) is recognized to respond to planetary scale teleconnections such as ENSO, NAO, and AO. In the positive phase of ENSO, namely El Nino condition, the north-south dipole mode in SAT appears over the tropical western Pacific and Japan, contributing to warm and dry conditions in southeast Asia and resulting in a weaker EAWM (Tomita and Yasunari 1996; Miyazaki and Yasunari 2007). Several studies have documented that the interannual and interdecadal variability of the NAO and AO induces the SAT variability in mid- and high-latitude Eurasia, including northern Japan. It is also known that the warming tendency in recent decades has been influenced by the positive trend of the NAO and AO on interdecadal timescales (Xie et al. 1999; Gong and Ho 2004, Thompson and Wallace 1999). As a new aspect of the EAWM, Wang et al. (2010) investigated that

there are two distinct modes in winter mean SAT variations. A northern mode that is associated with a cold winter in northern East Asia and results from cold air intrusions from central Siberia. In contrast, a southern mode that is associated with a cold winter south of 40°N resulting from cold air intrusions from western Mongolia. It is also found that the AO and Siberian High (SH), the contributing factors on EAWM circulation, are relatively independent of each other in influencing SAT variability over East Asia (Wu and Wang 2002).

b. Summertime Interannual Variability

The East Asia summer climate is associated with circulation anomalies of the Okhotsk high, subtropical Bonin (Ogasawara) high, and the Baiu/Mei-Yu stationary front between them (Kosaka and Nakamura 2010). These circulation anomalies control the East Asia Summer Monsoon (EASM) system. The appearance of the Okhotsk high tends to produce a cool summer in the northern part of Japan due to cold northeasterly wind, called 'Yamase', whereas an extension of the Bonin high results in a dry and hot summer in Japan (Yasunaka and Hanawa 2006). Few teleconnection patterns that affect the summer time climate over the Far East have been investigated (Wakabayashi and Kawamura 2004). The Pacific-Japan (PJ) pattern, one of the dominant summertime atmospheric teleconnection patterns, has been recognized as influential, given that anomalous convective activities over the tropical northwestern (NW) Pacific are highly correlated with the mid-troposphere circulation anomalies over East Asia (Nitta 1987; Kosaka and Nakamura 2008). In China, summer SAT anomalies are conveyed by the remote effect from the Tropical Indian Ocean (TIO) due to the meridional dipole circulation anomalies (Hu et al, 2011). The NW Pacific climate in summer following the

preceding winter ENSO conditions is highly correlated with Sea Surface Temperatures (SSTs) condition over the TIO, indicating the TIO warming as a capacitor for atmospheric anomalies over the Indo-western Pacific Oceans (Xie et al. 2009). Moreover, it is found that the ENSO's influence on the subtropical NW Pacific climate became more significant after the climate regime shift of the 1970s (Xie et al. 2010). Further examination of the PJ variability related to the ENSO on seasonal time scales is being investigated (Kosaka and Nakamura 2010).

1.4 Interannual Variability and SAT Extremes in Japan

Extreme SAT occurrences over East Asia are related to anomalous conditions of atmospheric circulations that control the East Asia SAT variability. The interannual variability of seasonal mean SAT at Tokyo in summer (JJA) and winter (DJF) season for 31 years since 1980 are shown in Figs. 1a and 1b, respectively. The interannual variability of winter seasonal mean SAT shows a quasi-decadal feature, which the variability is larger in 1980s and 2000s whereas it is relatively smaller in 1990s. Only taking account of the data period, both summer and winter variability has a linear warming trend, which might be partially influenced by urbanization around the Tokyo station.

As one of the extreme high SAT cases in East Asia, Japan has just experienced the hottest summer in 2010 (Fig. 1a). From the middle of July to September, many stations in Japan had daily mean temperature in excess of the 90th percentile of the distribution based on the last 31 years of data, which made a record of the highest seasonal mean temperature since observational records began in the late 19th century (Fig. 1c). The major contributing factor for the summer is considered as a strong influence of

the NW Pacific subtropical high, in addition to an influence of the preceding El Nino winter.

In contrast, 2005/06 winter season was one of the coldest winters for the data period in Japan (Fig. 1b). Beginning of middle of December, a month-long cold surge occurred, in association with several bomb cyclones around Japan (Inaba, 2010)(Fig. 1d). The cold air intrusion over warm ocean surface and mountain range caused the record-breaking snowfall in northeastern Japan, leaving nearly 150 fatalities and extensive power outages owing to this disaster. The subseasonal SAT variability was relatively large because of frequent extremes in both warm and cold temperatures, implying there were active synoptic transient eddies observed in the vicinity of Japan.

The summertime extreme hot days tend to persist from day to day, resulting in a shift of seasonal mean SAT (Fig. 1c), whereas the wintertime extreme hot and cold days have large daily variability, which contributes to a change in standard deviation of subseasonal SAT (Fig. 1d). This suggests that there are different mechanisms of influencing subseasonal SAT variability between summer and winter. Therefore, the temperature extremes on interannual time scales are influenced in two ways; a seasonal mean variability that shifts a mean of SAT distribution and a subseasonal variability that causes a broadening or narrowing of SAT distribution.

1.5 Objectives

It has been well established that the large-scale circulation and atmospheric teleconnection patterns of ENSO and AO have a regional scale effect on mean seasonal temperature over East Asia, by perturbing the East Asia monsoon system on intra-seasonal-to-interdecadal time scales. However, changes in the probability of temperature

extremes are more difficult to diagnose and understand than changes in mean climate. There has been little study of interannual variability of temperature extremes in terms of contributions of change in shape of probability distributions and also its physical climatic causes.

In association of large-scale circulation patterns, predictability of frequency in temperature extremes on interannual time scales would be further improved by investigating physical climatic causes that influence a shape of probability density distribution. Promisingly, regional and global atmospheric models should be able to produce the probability of SAT extremes on interannual time scales similar to those of observational data.

The purpose of this study is to investigate whether or not the interannual variability of SAT extremes over East Asia are dominated by seasonal mean variability or subseasonal variability of SAT distributions, in association with modes of large-scale climate variability. Mechanisms of extreme daily SAT occurrences in winter and summer are examined, in terms of spatial distributions of the extremes and their physical climatic variables that control the probability of extremes.

CHAPTER 2

DATA AND METHODS

2.1 Data

The daily mean SAT, pressure reduced to mean sea level (MSLP) and surface 10-m wind are derived by taking a daily mean of 6 hourly data from 1979 to 2010, obtained from the Japanese 25-year ReAnalysis (JRA-25, Onogi et al. 2007), which are gridded on a 1.1° latitude-longitude grid. Monthly mean temperature, wind, downward solar radiation flux, and geopotential height at the surface, 925 hPa, and 500 hPa are also obtained from the JRA-25. The Climate Prediction Center (CPC) Merged Analysis of Precipitation (CMAP, Xie and Arkin 1997), National Oceanic and Atmospheric Administration (NOAA) Interpolated Outgoing Longwave Radiation (OLR, Liebmann and Smith, 1996), and NOAA extended reconstructed Sea Surface Temperature (SST) V3b are used for monthly precipitation, OLR, and SST from 1979 to 2010, respectively. They are gridded on 2.5° latitude-longitude grid. Monthly global gridded high-resolution (0.5° latitude-longitude grid) station data for precipitation and surface air temperature are obtained from the UDel_AirT_Precip (http://www.esrl.noaa.gov/psd). Cloud amount data, a gridded satellite-derived data, is obtained from the International Satellite Cloud Climatology Project (ISCCP) for the period from 1983 to 2001.

As in the definition of the mid-latitude storm tracks, time periods of fluctuations associated with migratory synoptic scale disturbances are typically shorter than a week (Nakamura and Wallace, 1990 and Nakamura, 1992). The eddy kinetic energy (EKE) is a product of summation of squared u and v components at the 500-hPa level (i.e.,

$\frac{1}{2}[u'^2+v'^2]$), where the u' and v' are high-pass filtered time series with a cutoff period of 9 days.

The winter season is defined as December-February (DJF) and summer as June-August (JJA). The winter year is defined by that of January and February. February 29th in leap years has been removed so that each winter season has the same number of calendar days. I define East Asia region as regions extending from 90°E to 160°E and from 20°N to 60°N. The domain covers China, Mongolia, south-southeastern Russia, Korea, and Japan. The domain also includes the leeward region of the Tibetan Plateau, and parts of the northwest Pacific, East and South China Sea, and Sea of Okhotsk. The surface geometric height in the reanalysis model takes account of the Himalayan mountain range, Tibetan plateau, and Mongolian basin (Fig. 2).

2.2 Methods

a. Definition of Extreme

All SAT values are presented as anomalies after the removal of the seasonal cycle. To define a seasonal cycle, I firstly applied a simple calendar day mean by averaging daily mean SAT for each of the 365 days in the 31-year period since 1979. However, the shortness of the record results in substantial high-frequency noise by simple averaging (black line in Fig. 3). In order to produce a smoother seasonal cycle, I applied two different methods, harmonic smoothing and moving-average smoothing. For the former method, I retain the first four harmonics of the seasonal cycle. The cycle is smoothed well except for August where the smoothed cycle exceeds most calendar day mean in roughly calendar days 210-230 (blue line in Fig. 3). To produce a smoothed without such bias, I use a 21-day (i.e., preceding and following 10 days) moving average

for the entire period to remove large fluctuations in daily mean temperatures. The 21-day smoother is chosen because most weather systems have a lifetime shorter than 2-3 weeks in mid-latitudes. The seasonal cycle obtained by the 21-day moving average sufficiently represents an annual cycle (red line in Fig. 3).

Once the time series of daily mean SAT anomalies for both seasons are obtained by removing the annual cycle, I calculate the number of cold and warm extreme days for each season. Daily mean cold (warm) temperature extremes are defined as those in the lower (upper) 10^{th} percentile of the climatological distribution of daily mean SAT at each grid point and station. Seasonal mean SAT and subseasonal SAT deviation is defined by taking a mean and standard deviation of the daily mean SAT anomalies for each season, respectively.

b. Large-Scale Circulation Index

I obtained the monthly mean Arctic Oscillation (AO) index and Southern Oscillation index (SOI) from the NOAA/CPC. The AO pattern is defined as the leading Empirical Orthogonal Function (EOF) of monthly mean Northern Hemisphere sea-level pressure for all months of the year during 1979-2000 (Thompson and Wallace 1998). AO index is the normalized leading principal component (PC) time series. The SOI is a normalized time series of difference in monthly mean sea-level pressure anomalies between Tahiti and Darwin (Ropelewski and Jones, 1987). The monthly mean East Asia winter monsoon index (MOI) is derived by taking the sea level pressure difference between Irkutsk, Russia and Nemuro, Japan, which are the closest cities with available station data to the center of Siberian High and Aleutian Low, respectively (Matsumura and Xie, 1998). It is often used to examine winter monsoon strength over East Asia. The

Pacific-Japan (PJ) teleconnection is defined by the leading EOF of monthly 850-hPa vorticity anomalies over the domain of 0°-60°N and 100°-160°E and the monthly mean index is its normalized leading PC time series (Kosaka and Nakamura 2010). All indices are normalized by subtracting the mean and dividing by the standard deviation. A positive year is defined when the index is 0.5 or above, whereas a negative year is defined when the index is -0.5 or below. A neutral year is defined when the index is within ±0.5.

c. Probability Density Function

For graphical representation of distribution of data, histograms of daily mean temperature are smoothed by kernel density function to construct the smoothed Probability Density Function (PDF). The kernel density estimator *f* is defined as

$$f(x) = \frac{1}{nh}\sum_{i=1}^{n} K\left(\frac{x - x_i}{h}\right) \quad \text{where} \quad K(x) = \frac{1}{\sqrt{2\pi}} e^{-\frac{1}{2}x^2} \qquad \text{eq. (1)}$$

where *K(x)* is the Gaussian kernel and *h* is a smoothing parameter called the bandwidth. Normal kernels with a certain variance on each of the data point x_i are summed to make the kernel density estimate. Thus, the kernel density estimate is non-parametric way of estimating the PDF of random variable, whose smoothness well visualizes the distribution of data compared to the discreteness of histograms.

CHAPTER 3

RESULTS FOR WINTER

3.1 Climatology

Climatological mean SAT and its variation are important to examine from the viewpoint of frequency distribution of SAT related to extreme temperature values. Climatological mean and standard deviation of SAT are derived based on seasonal daily mean SAT data. The stationary anticyclone/cyclone pair, the Siberian High and Aleutian Low, generates dominant northerly surface winds over East Asia, with maximum strength over the ocean in mid-latitudes (Fig. 4a). The SAT gradient is large along the Himalayan mountain range due to the elevation. It is also large 25°N in SE China through 40°N in the NW Pacific and 40°N in the continental East Asia. There is a smaller SAT gradient in the eastern plain between Yellow and Yangtze River basins (Figs. 4a-b).

In general, the standard deviation of SAT on interannual time scales gradually decreases from high- to low-latitudes monotonically. The distribution of subseasonal SAT deviation, however, differs from that of the interannual variability in winter. It is interesting to note that the subseasonal SAT variability in SE China, N-NE China, and the northern Japan Sea through the eastern region offshore of Japan is relatively higher than surroundings, where the climatological SAT gradient is large as well (Fig. 4b). Moreover, it is evident that the higher the elevation, the smaller the subseasonal SAT deviation, especially seen in the Tibetan Plateau (Fig. 4c). In order to identify what causes the larger subseasonal SAT deviation in mid-latitudes, I superimpose the climatological EKE over the SAT variability (Fig. 4c). There are two major axes of storm tracks, one extending from the Korea Peninsula to northern China and another extending from the East China

Sea through SE China. The large SAT deviation corresponds to the larger variability of meridional heat transport by active transient eddies, resulting in/from the large climatological SAT gradient.

As a summary of the regional variability in climatological subseasonal SAT variability, the large variability in mid-latitudes, including N-NE China through the eastern region offshore of Japan, is caused by active mid-latitude cyclones, which coincide with the larger climatological SAT gradient. Similarly, the large subseasonal SAT deviation and the concentrated SAT gradient are seen in SE China, resulted from storm activity related to the East Asia subtropical jet. Cold surges from mid-latitude weather systems and warm air advection from both mid-latitude and tropical weather systems could also impact the higher subseasonal SAT deviation in this region. The large SAT subseasonal variability in the Sea of Okhotsk results from the large interannual variability of initial sea ice formation and extent, which is mostly determined by a preceding fall heat flux over the northwest Sea of Okhotsk (Ohshima et al 2006). In this region, the interannual variability of SAT is similar to its subseasonal SAT variability because SAT is strongly influenced by the surface heat flux due to ocean and sea ice, which has a large interannual variability, but small subseasonal variability.

3.2 Interannual Variability

a. Empirical Orthogonal Function (EOF) Analysis

In order to examine the interannual variability of East Asia SAT and extreme SAT occurrences, Empirical Orthogonal Function (EOF) analysis is applied to anomalies of seasonal mean SAT [i.e., $\mu'(SAT)$], subseasonal SAT deviation [i.e., $\sigma'(SAT)$], and seasonal frequency of cold and warm temperature extremes. The anomalies are weighted

by the square root of cosine latitude to ensure the correct geographical proportion before applying EOF analysis. The spatial patterns of the first two leading modes and corresponding percentage of the total explained variance for each variable are shown in Fig. 5.

The leading EOF of seasonal mean SAT, which explains 36% of the total variance, is a monopole pattern with the largest interannual variability over Siberia and NW Sea of Japan and troughs extending to eastern China and NW Pacific (Fig. 5a). This mode correlates with the AO index at 0.58 (Table 1a) and with the MOI at -0.73 (Table 1b), which are statistically significant at the 99% level. In contrast, the second EOF of seasonal mean SAT shows a north-south dipole pattern with an axis at 35°N to 45°N and explains 22% of the total variance. This dipole mode correlates with the AO index at 0.36 (Table 1c) and the SOI at -0.35 (Table 1d), which are statistically significant at the 90% level.

Regarding the relationship between the AO and monsoon circulation being primarily driven by Siberian High (SH) variability, it is found that AO and SH are relatively independent of each other in influencing the SAT variability over East Asia despite that they are correlated statistically significant. Impacts of the SH occur primarily southwards of 50°N, the NW Pacific and the South China Sea, because the AO suppresses the SH's influence on the high latitudes of the Asian continent and the some subarctic regions (Wu and Wang 2002). Thus, the monsoon variability is correlated with the AO at -0.42, resulting in the large correlation of the first EOF of seasonal mean SAT with the AO at 0.58 and MOI at -0.78 (Table 1).

The first and second EOFs of subseasonal SAT variability show monopole and meridional dipole patterns, explaining 28% and 16%, respectively (Figs. 5c-d). The PC1 of subseasonal SAT deviation is highly correlated with the PC2 of seasonal mean (Table 1e) and also significantly correlated with the AO index (Table 1f). Although the PC1 of seasonal mean and PC2 of subseasonal SAT deviation do not have a strong relationship (Table 1g), the former is correlated with the MOI at -0.73 (Table 1b) and the latter at 0.38 (Table 1h).

EOF analysis is also applied on the annual frequency of cold extreme occurrences (CEO) and warm extreme occurrences (WEO) in order to examine interannual variability of extreme occurrences. The leading EOF of both CEO and WEO features a monopole patterns (Figs. 5e-f) while the second EOFs have a North-South dipole patterns (Figs. 5g-h); both are spatially consistent with the corresponding EOFs of seasonal mean SAT (Figs. 5a-b). As shown within the bolded block in Table 1, the correlation coefficients between seasonal mean SAT and SAT extremes on PCs indicate that both CEO and WEO are significantly correlated with seasonal mean SAT variability.

b. Linear Regression Analysis

Interannual variability of large-scale atmospheric circulation pattern and associated anomalies of seasonal mean SAT and subseasonal SAT deviation are examined in linear regression. The regression analysis is applied to circulation anomalies near surface and in the upper air with the MOI and AO variability.

In strong monsoon years, there is a large negative mid-troposphere height anomaly centered over Japan and a positive anomaly in northwestern Russia (Fig. 6b). This indicates a large Rossby wave train, resulting in the deepening of the East Asian

major trough, the southward shift of the East Asian jet relative to its climatology, and the intensified westerly south of 40°N. Corresponding to the upper air circulation anomaly, a cold SAT occurs from Siberia to the rest of the East Asia region south of 50°N except for the down slope side of the Tibetan plateau. This cold SAT anomaly pattern associated with the monsoon variability corresponds to the southern mode discussed in Wang et al (2010), which is associated with a cold winter south of 40°N resulting from cold air intrusions from western Mongolia. It also agrees with that a significant influence of the monsoon on seasonal mean SAT is only seen south of 40°N over Japan (Matsumura and Xie 1998, Xi and Noguchi 1999). Associated with the strong monsoon variability, the subseasonal SAT variability shows a spatially patchy distribution (Fig. 6c). It becomes larger in Gobi Desert region and south of Japan and smaller in part of eastern Russia and northern Japan. The larger subseasonal SAT variability seems to correspond to the intensified westerly and southward shift of the upper-level polar jet. The larger SAT variability just south of Japan is consistent with that storm track shifts southward when the monsoonal circulation is intensified, resulting in larger daily mean SAT variations along the intensified storm track (Nakamura et al, 2002).

For the AO variability, regression analysis is applied with the negative phase of AO (i.e., opposite sign of the AO index) in order to examine cold temperature cases over East Asia in winter. During the positive phase of the AO, surface pressure is anomalously low in the polar region. This helps the mid-latitude jet stream to blow strongly and consistently from west to east, thus keeping cold Arctic air locked in the polar region. In contrast, the negative phase of AO is associated with anomalous high pressure in the polar region, weaker zonal winds between 50°N and 70°N, and greater meridional

intrusion of polar air into mid-latitudes, including northern Japan (Figs. 7a-b) (Thompson and Wallace 1999, Xie and Noguchi 1999). The subseasonal SAT deviation becomes larger significantly from the Siberia to NE China, which is consistent with the intensified upper-level polar jet that result in more meridional heat transports by active storm activities (Fig. 7c).

c. Physical Cause

It is shown that mode of the monsoon and AO variability significantly influences seasonal mean SAT anomalies over East Asia (Figs. 6a and 7a). These anomalies are associated with advections of the climatological SAT gradient by anomalous surface wind, which is expressed as $\mu(T') \propto U' \cdot \nabla T$. Thus, temperature advections cause the interannual variability of SAT over East Asia in winter. In contrast, the subseasonal SAT anomalies associated with the mode of the monsoon and AO variability seem to be significant in regional scales (Figs. 6c and 7c). This seems to link meridional heat transports by storm activity, which is expressed as $\sigma(T') \propto \sigma(v')\frac{\partial T}{y}$. Thus, subseasonal variability of surface meridional wind over the climatological SAT gradient is a mechanism for the interannual variability of standard deviation of subseasonal SAT.

c. Extreme Temperature Occurrences

In order to extract the interannual variability of CEO and WEO, I apply regression analysis of the MOI and AO index with the frequency of cold and warm extremes that exceed the lower and upper 10^{th} percentile of the climatological SAT at each grid point. In addition, I perform a summation of the CEO and WEO regression coefficients to examine asymmetries in amplitude between cold and warm extremes. Under the

assumption of Gaussian distributions, which is a reasonable approximation in many locations, one may argue that asymmetries between cold and warm extremes would arise when shifting a mean of the distribution without changing its shape and also when changing a shape of the distribution through broadening or narrowing. For instance, an increase in seasonal mean SAT will increase warm extreme days more than decreases cold extreme days. However, instead of examining whether or not an anomaly of mean SAT would influence to extreme occurrences, we would like to know how an oscillation of mean SAT would influence to extreme occurrences on average. For a Gaussian distribution, the regression/correlation of extreme occurrence anomalies should be symmetric between cold and warm extremes when the data include multiple cycles of the oscillation. Thus, significant asymmetries of regression coefficients between cold and warm extremes provide regions where not only shifts a seasonal mean, but also changes standard deviation of subseasonal SAT, which would decrease or increase the number of extreme days.

In strong monsoon years, the number of cold days increases significantly from western Mongolia to 40°N south around Korea and Japan (Fig. 8a), whereas that of warm days decreases from Siberia to Japan (Fig. 8b). Negative asymmetry extends from Siberia to NE China and northern Japan, whereas positive asymmetry extends from SE China to southern Japan (Fig. 8c). The spatial characteristics of the asymmetries are similar to that of regression on subseasonal SAT variability with MOI (Fig. 6c), which suggests the influence of subseasonal SAT variability onto extreme SAT occurrences.

In contrast, the increase in the number of cold days mainly occurs north of 35°N in the negative phase of AO (Fig. 9a) and the decrease in the number of warm days

occurs from Siberia to Japan (Fig. 9b). Significant asymmetries are centered near Irkutsk, the Gobi Desert, and NE China (Fig. 9c). This spatial pattern of the asymmetry corresponds to that of subseasonal SAT variability, which is regressed with the negative phase of AO (Fig. 7c). Therefore, the asymmetry between CEO and WEO in the linear regression analysis of the AO variability explains the anomalies of subseasonal SAT variability.

3.3 Frequency Distribution

For further investigation in influence of seasonal mean SAT and subseasonal SAT variability on extreme days, I calculate histograms of the daily mean SAT anomalies for the AO and monsoon variability and smooth them by using the Kernel density estimation. In Fig. 10, the upper panels in each figure show the distributions with means of each mode and the lower panels show the distributions without means of each mode. Hence, the distributions in the lower panels explain the subseasonal SAT distribution without seasonal mean effects. I choose the station at Harbin in northeast China (Fig. 2), where extreme occurrences are significantly correlated with the AO and monsoon variability in winter.

In the negative phase of AO, the seasonal mean SAT decreases, resulting in more cold extreme days and fewer warm extreme days (upper panel in Fig. 10a). However, the standard deviation of subseasonal SAT variability becomes larger at the same time, resulting in the increase in both the cold and warm extreme days (lower panel in Fig. 10b). Thus, the negative phase of AO results in more increases in cold extreme days than decreases in warm extreme days (Upper panel in Fig. 10a), causing the asymmetric change between cold and warm extremes (Fig. 9c). The distributions using station data

confirms the similar seasonal mean shifts, but the uncertainty in terms of change in the shape of distributions (Fig. 10b).

In contrast, the standard deviation of subseasonal SAT variability becomes smaller (lower panel in Fig. 10c), causing the reduction of both cold and warm extreme days, in strong monsoon years when the seasonal mean SAT largely decreases. Hence, there are fewer increases in cold extreme days than decreases in warm extreme days in the strong monsoon years (upper panel in Fig. 10c). Carefully looking at the distribution of strong monsoon years, both upper and lower tails becomes narrower, contributing to smaller standard deviation and influencing the number of extreme days in the lower and upper 10^{th} percentiles (lower panel in Fig. 10c). Distribution of station data shows the same narrowing effect on both tails (lower panel in Fig. 10d).

The SAT distributions for the AO mode and the monsoon variability at Harbin is a good example that the cold (negative) phase of AO is associated with broadening of subseasonal SAT variability whereas the strong (positive) phase of monsoon is associated with narrowing of subseasonal SAT variability. This type of SAT distributions is evident north of 43°N (Figs. 8c and 9c). In contrast, the SAT distributions at Beijing in China show that both the negative (cold) phase of AO and the positive (strong) phase of monsoon are related to the broadening of subseasonal SAT variability, resulting in increasing cold extreme days more than decreasing warm extreme days (Fig. 11). In the distributions of Beijing, it is confirmed that the reanalysis data reproduce the changes in mean of the distributions similar to that of station data overall. However, the changes in shape of distributions, namely the standard deviation, skewness, and peak of the distribution, are uncertain between the reanalysis data and station data.

CHAPTER 4

RESULTS FOR SUMMER

4.1 Climatology

Summertime (JJA) climatological SAT spatial pattern is examined (Fig. 12). There are two anticyclonic flows associated with the subtropical NW Pacific high and the Okhotsk high (Fig. 12a). The SAT gradient is large between the warm-moist air mass of Ogasawara (Bonin) and the cool-moist air mass of Okhotsk. The monsoonal southerly causes warm air advection through NE China. The downward shortwave radiation flux is large in the Gobi desert and small over the east region offshore of northern Japan, which is linked to storm tracks (Fig. 12b). Minimum region of total cloud amount in the Gobi Desert seems to correspond to the warmer SAT (Fig. 12c). In contrast, maximum cloud amount in the NW Pacific is along the northern flank of the upper-level jet (Figs. 12c and 13a).

The subseasonal SAT variability, the standard deviations of subseasonal SAT, is also examined. Compared with surroundings, it is larger about 40°N from the northern Japan to its east, corresponding to the storm activity (Fig. 13a). The maximum SAT variation is apparent in the northern Mongolia. The Gobi desert is a rain shadow desert formed by the Himalaya range blocking rain-carrying clouds from reaching the Gobi from the Indian Ocean. Due to the extreme low moisture, larger downward solar radiation with clear sky, and the low heat capacity of its surface, the daily-to-interannual variability of SAT is very large in the high-altitude region. Consequently, the standard deviation of subseasonal SAT is similar to that of the interannual SAT variability during summer.

For further investigation into the large subseasonal SAT variability in Mongolia, I examined climatological storm tracks and precipitation. Diurnal variations of convective activity in Ulaanbaatar, Mongolia, were examined, which was tied to soil moisture conditions rather than to the diurnal variation of precipitable water associated with thermally induced local circulation (Iwasaki et al, 2008). This suggests positive/negative feedbacks between soil conditions and rainfalls. For instance, in moist soil conditions, an increase in water vapor in the boundary layer due to evapotranspiration will lead led to potentially unstable condition. This sustains deep convective activities in addition to orographic convergence. As a result, more rainfall keeps soil condition more saturated. A feature is opposite in the dry soil conditions. Thus, the large subseasonal SAT variability in Mongolia might be linked to intra-seasonal or seasonal mean precipitation variability. The subseasonal SAT center is over the northern Mongolia, located on the northern edge of the Gobi desert (Fig. 13a). It is also on the southern flank of a mid-latitude wet zone and northern flank of the westerly jet north of the Tibetan Plateau (Fig. 13b). Thus, the precipitation and storm activity are the main reasons for the large subseasonal SAT variability.

4.2 Interannual Variability

a. EOF Analysis

Similar to the winter case, I firstly applied EOF analysis to the summertime (JJA) seasonal mean SAT, standard deviation of subseasonal SAT, and the number of cold and warm extreme days in order to extract the leading modes of interannual SAT variability.

The leading EOF of seasonal mean SAT, [μ' *(SAT)*], which explains 28% of the total variance, is a monopole pattern with maximum loadings over the southern Siberia,

Mongolia, and NE China (Fig. 14a). This mode correlates with the preceding winter (NDJF) SOI at 0.41 (Table 2a), which is statistically significant at the 90% level. The simultaneous correlation between JJA seasonal mean SAT and SOI (JJA) does not show a significant relationship (not shown). The second EOF of seasonal mean SAT is a meridional tri-pole pattern with maximum loadings over the Philippine Sea, region from the Japan Sea to northern Japan, and the northeastern Siberia, and explains 22% of the total variance (Fig. 14b). This tri-pole pattern is correlated with the PJ index at 0.67 (Table 2b), which is statistically significant at the 99% level. This mode is also correlated with the preceding winter SOI at 0.36, but not with the simultaneous SOI. However, the PJ index is correlated with SOI (-NDJF) and SOI (JJA) at 0.46 and 0.37, respectively, which are statistically significant at the 90% level. Thus, the second mode of seasonal mean SAT indicates the PJ-like variability, which has an atmospheric teleconnection from the west rather than direct influence from SST conditions in the tropical Pacific.

Because the characteristics of SAT and rainfall variability over East Asia in summer differ between June and August, I split the summer season into the first half period (i.e., June 1 - July 15) and the second half period (i.e., July 16 - August 31) and apply an EOF analysis in a similar way. The results show that the first two leading modes of seasonal mean SAT are dominated in the first half period during the Meiyu/Baiu rainfall season (not shown).

The first EOF of standard deviation of subseasonal SAT, [σ' *(SAT)*], explaining 14% of the total variance, is also a monopole pattern with maximum loadings in Mongolia (Fig. 14c) during the second half of summer season. In contrast, the second EOF of subseasonal SAT has an interesting spatial distribution that explains 12% of the

total variance, in which the primary center of action is located along the Mei-Yu/Baiu rain band and anomalies of opposite sign are over the Siberia and the NW Pacific (Fig. 14d).

EOF analysis is also applied to summertime seasonal CEO and WEO. The first EOFs of both CEO and WEO have distributions similar to those of the first EOF of the seasonal mean SAT (Figs. 14e-g) and both correlate with the PC1 of seasonal mean SAT at 0.93 and 0.96, respectively, which are statistically significant at the 99% level (Table 2e, f). As shown within the bolded block in Table 2, it is apparent that both the CEO and WEO are dominated by seasonal mean SAT (Table 2e, f), but only WEO is correlated with the subseasonal SAT deviation on the first PCs (Table 2h). In contrast, the second PC of CEO is correlated with the subseasonal SAT deviation than the seasonal mean SAT (Table 2i), whereas the second PC of WEO is dominated by the seasonal mean rather than the subseasonal SAT deviation (Table 2g).

b. Linear Regression Analysis

In this section, the linear regression analysis is applied to climatic variables near surface and in the upper air with the preceding SOI and summertime PJ index on interannual variability.

Anomalies in summer associated with the preceding La Nina winter are shown in Figs. 15-17. During the summer after a La Nina winter, the 500-hPa geopotential height anomaly shows anomalous cyclones in the subtropical Indo-Pacific regions, which is associated with active convective activities, and anomalous anticyclones in regions 40°N-55°N of East Asia, due to the Rossby wave response (Fig. 15b). Seasonal mean SAT increases in Mongolia through NE China, northern Japan, and its east, where surface

warm air advections are confirmed (Fig. 15a). In addition, associated with the anomalous anticyclonic height in the mid-troposphere, synoptic scale subsidences contribute to an increase of clear sky days, which increases the downward solar radiation flux and results in warmer seasonal mean SAT (Fig. 16a). Indeed, the seasonal mean cloud amount decreases throughout the East Asia except for the SE China (Fig. 16c). There are less cloud amount, more downward solar radiation, and higher SST just south of Japan in the NW Pacific, despite the maximum SAT response in eastern regions of the northern Japan. This suggests that warm air advection may also contribute to the northward shift of SAT response (Figs. 15a and 16). Precipitation tends to decrease over the region from Mongolia to NE China, resulted in the increases in the seasonal mean SAT, and SSTs corresponding to warmer SAT in the NW Pacific near northern Japan (Fig. 16b).

Anomaly of standard deviation of subseasonal SAT associated with the preceding winter La Nina is examined (Fig. 17). The storm track, defined as an axis of the mid-troposphere 500-hPa eddy kinetic energy, shifts northward relative to its climatology position, associated with the intensified westerly flow north of 50°N (Figs. 15b and 17a). The storm activity is suppressed between 25°N and 45°N corresponding to a decrease in precipitation (Fig. 17a). Regional decrease in subseasonal SAT standard deviation in the east coast of China and the southern coast of Japan are due to the minimum of storm activities (Fig. 17b). In contrast, significant increase of subseasonal SAT variation in Mongolia is along the axis between positive and negative storm anomalies as well as precipitation anomalies (Figs. 17a-b). This suggests that the subseasonal SAT variability is influenced by both the precipitation and storm activity in Mongolian region.

As the second leading EOF of JJA seasonal mean SAT, the linear regression associated with PJ pattern is examined in the rest of the section. In the positive phase of the PJ, convective activity is intensified in the subtropical NW Pacific. Through the atmospheric teleconnection, an anticyclone anomaly in mid-troposphere is around Japan and a cyclonic anomaly is centered near the Sea of Okhotsk (Fig. 18b). The seasonal mean SAT and SST variability are explained by the variability of downward solar radiation associated with synoptic scale circulation and total cloud amount anomalies (Fig. 19). Even though there is no significant SAT response over the ocean south of Japan, the less cloud amount and more solar radiation are confirmed. In this region, surface wind anomaly is easterly, which is parallel to the climatological SAT gradient (Fig. 18a). This suggests the importance of warm air advection in influencing the SAT variability. In fact, a seasonal mean SAT increases significantly in the Japan Sea, where less cloud amount, more solar radiation flux, warm SST, and southerly surface wind are confirmed (Figs. 18a and 19). Standard deviation anomalies of subseasonal SAT, which are statistically significant at the 90% level, are spatially patchy distributions in the PJ variability (Fig. 20b). The storm track is shifted northward with its center in the northern Japan, corresponding to the intensified westerly (Fig. 18b and 20a). The opposite feature is evident from the eastern China to southern Japan. The subseasonal SAT standard deviation is relatively small around Shanghai, the Korean Peninsula, and southern Japan, which are explained by less active storm tracks. Less amount of precipitation results in less variations of daily mean SAT (Figs. 20a-b).

c. Extreme Temperature Occurrences

Interannual variability of the number of cold and warm extreme days is examined by linear regression analysis on the ENSO and PJ variability. Similar to the winter extreme cases, asymmetries between CEO and WEO regression coefficients are also analyzed.

In the southern oscillation variability, the spatial distributions of the CEO and WEO, which are statistically significant at the 90% level, correspond to the SAT anomaly between 40°N and 55°N over East Asia (Figs. 21a-b). The spatial distribution of significant asymmetry is similar to that of subseasonal SAT variability in Mongolia, the eastern coast of China, and the southern coast of Japan (Figs. 21c and 17b).

In the PJ variability, the spatial distribution of the CEO and WEO is also consistent with seasonal mean SAT anomaly (Figs. 17a-b). It is noteworthy that significant WEO only occurs in Korea, the Sea of Japan, and northern Japan (Fig. 22b). In contrast, significant CEO occurs in the Yellow Sea and the central-to-northern Japan (Fig. 22a). Significant asymmetries are localized with its maximum/minimum asymmetry in the eastern Mongolia, eastern coast of China, the Sea of Japan, and south of Japan (Fig. 22c), showing similar to the spatial pattern of the subseasonal SAT variability (Fig. 20b).

4.3 Frequency Distribution

Smoothed histograms of the daily mean SAT anomalies related to the ENSO and PJ interannual variability are examined, using both the reanalysis and station data from Ulaanbaatar, Mongolia and Shanghai, China.

For Ulaanbaatar in Mongolia, a mean of the SAT distribution increases and standard deviation of the distribution becomes larger during summer after a La Nina winter (Fig. 23a). Thus, it results in the increase in the number of warm extreme days

more than the decrease in the cold extreme days. The distributions based on the station data are similar to that of the reanalysis data only from a viewpoint of the mean shift and narrowing/broadening of the standard deviation (Fig. 23b). Anomalies of the seasonal mean and standard deviation of SAT distribution associated with the PJ variability do not show significant changes since the SAT variability in Mongolia is not significantly influenced by the PJ teleconnection pattern (Figs. 23c-d).

For Shanghai in China, the climatological SAT distribution is unique with its shape (Fig. 24). Associated with both the ENSO and PJ variability, seasonal mean shifts are not significant. However, standard deviations between positive and negative phases show a narrowing and broadening of the distributions, which influences the number of extreme days, to some degree. For instance, in the positive phase of the PJ summer after a La Nina winter, the distributions narrow with a reduction in extreme days. Only in terms of variance changes, distributions based on the reanalysis data are similar to that of the station data. Influences of seasonal mean shift onto the number of extreme days are somewhat difficult to be detected in the SAT distribution at Shanghai.

CHAPTER 5

CONCLUSION

5.1 Summary

In this study, the interannual variability of seasonal mean SAT and subseasonal SAT variations over East Asia are investigated in order to analyze physical causes for extreme temperature occurrences in relation to large-scale circulation anomalies. The results of EOF and regression analysis of seasonal mean SAT, standard deviation of subseasonal SAT, and the number of cold and warm extreme days, reveal that a seasonal mean shift in probability distribution is the dominant factor that influences the number of extreme days. There is also a regional influence of subseasonal SAT variations on extreme days, which is explained by asymmetries of regression coefficients between the number of cold and warm extreme occurrences. In an examination of the frequency distributions of daily SAT anomalies associated with mode of climate variability, the reanalysis data could approximately produce the major mean shifts and changes in standard deviation of the distributions that occur in the station data at particular stations such as Harbin, Beijing, Shanghai in China, and Ulaanbaatar in Mongolia. Such comparisons between frequency distributions of other stations of Irkutsk in Russia, Chengdu and Shanghai in China, and Sapporo and Tokyo in Japan, also reveal the similar robustness but not presented here.

In winter, a seasonal mean shift of the daily SAT distributions is a dominant factor that influences the number of cold and warm extreme days. The seasonal mean SAT anomaly is determined by the advection of the climatological SAT gradient by anomalous surface winds. Moreover, the results show that the number of SAT extremes

is also influenced by subseasonal SAT variations. In both the AO and East Asia winter monsoon variability, synoptic-scale transient eddies are modulated in association with anomalous westerly in mid-troposphere. Meridional heat transports by active transient eddies seem to be a mechanism for subseasonal SAT variations. Hence, when the storm track is more active, the subseasonal standard deviation of SAT becomes larger. In addition to the storm activity, the subseasonal SAT variation is also influenced by the frequency of cold Arctic air intrusion from higher latitudes related to the daily and seasonal variability of the AO.

In summer, a seasonal mean shift of daily SAT distribution is a major cause for extreme temperature occurrences in both the preceding winter ENSO and PJ variability. Variability of downward shortwave radiation flux, which is associated with cloudiness due to anomalous mid-troposphere height, seems to control the seasonal mean temperature. In addition, significant SAT response is also related to cold/warm air advection. Subseasonal SAT variations, which are explained by storm activity, also influence the SAT extremes in particular regions. In Mongolia region, the large subseasonal SAT variability seems to be controlled by both precipitation and storm activity.

5.2 Discussion

a. Histograms

The analysis has done based on the gridded reanalysis data in order to examine the large-scale features of extreme SAT occurrences. I have examined the station data by plotting smoothed histograms of each mode of climate variability only for several locations including Irkutsk in Russia, Ulaanbaatar in Mongolia, Harbin, Beijing, and

Shanghai in China, and Sapporo and Tokyo in Japan. Comparisons between the reanalysis and station data for more locations would help to understand more insight of extreme occurrences. However, it is only discussed that the results from the smoothed histograms show how seasonal mean shifts and changes in standard deviation would change the number of extreme days under the assumption that it is the Gaussian distribution. In reality, anomalous SAT distributions for mode of climate variability and its climatological distributions at each locations are much more complex. For instance, the distributions shown in this study proves that not only mean and standard deviation, but also skewness and kurtosis of the distributions also influence the changes in shape of distributions.

b. Trend Effect

Because of the shortness of the data period, linear trends or long term trends were not removed from the raw data in this study. However, temperature globally increases at a rapid rate in this data period. Indeed, the linear trends of winter and summer seasonal mean SAT at Tokyo show warming trends at the rate of 0.4°C and 0.6°C per decade, respectively (Figs. 1a-b). This would result in more warm extreme days and less cold extreme days in the latest decade than those in 1980s. Thus, the question that arises when viewing the warming trend is how the long-term trend influences the number of extremes at times. The analysis without the trend effects would be necessary in order to examine how the short term linear trends contributes to the number of extreme days in the last three decades. Moreover, such a strong warming trend at Tokyo station might be resulted from urbanization effects. The station records indicate that there is a strong warming trend in the center of Tokyo, whereas the surrounding cities do not have such a rapid

trend. Thus, this kind of effect need to be considered when analyzing the interannual variability of extreme occurrences, which is linked to large-scale climate variability.

c. Definition of Extremes

In this study, I define the extreme SAT occurrences as the number of days in excess of the lower and upper 10^{th} percentiles of climatological daily mean SAT distributions. However, extreme SAT occurrences are, in general, considered as each extreme SAT event, which may usually be a sequence of days that exceed a certain threshold value. For instance, an extreme hot SAT event in 2010 summer in Japan is a good example. During the period, a nearly month-long heat wave resulted in a series of days exceeding the 90^{th} percentile of the climatological daily mean SAT distribution (Fig. 1c). Therefore, it would be more beneficial to analyze extreme temperature occurrences by taking account of the number of extreme SAT events instead of extreme SAT days. In addition, a selection of threshold for more extreme values such as 95% and 99% of the climatological distribution is another way to define extreme SAT occurrences. This would lead rare extreme events that may occur once in a few or decadal years. Taking advantage of GEV distributions would be helpful when analyzing the most extreme SAT occurrences.

d. Predictability

Interannual variability of extreme SAT occurrences is examined in relation to modes of large-scale climate variability in this study. Because the results reveal that seasonal mean SAT dominantly influences the number of extreme days over East Asia and subseasonal SAT variation partially contributes to the extreme days in particular region, the number of SAT extreme days on seasonal time scales could be somewhat

predictable, depending on predictability of large-scale circulation anomalies. For example, with a focus on the summer following the mature phase of El Nino, models are overall successful in predicting NW Pacific atmospheric anomalies during summer, being identified as influential on seasonal mean SAT variability in East Asia (Chowdary et al, 2010). In contrast, it is more challenging to forecast the winter seasonal SAT variability in the leading months because of the difficulty in predicting the AO on intra-seasonal and interannual time scales. Therefore, if the predictability of large-scale climate variables is improved and its relation to SAT variability is furtther understood, this study would benefit modeling the interannual variability of extreme temperature occurrences.

REFERENCES

Ballester, J., Giorgi, F., Rodo, X., 2010: Changes in European temperature extremes can be predicted from changes in PDF central statistics. *Climate Change*, **98**, 277-284

Beniston, M., Stephenson, D.B., 2004: Extreme climatic events and their evolution under changing climatic conditions. *Global and Planetary Change* **44** (2004) 1-9

Chang, C.-P., Wang, Z., Hendon, H., 2006: The Asian winter monsoon. *The Asian Monsoon*, Wang, B. Ed., Praxis, 89-127

Chowdary, J.S., Xie, S.-P., Lee, J.-Y., Kosaka, Y., Wang, B., 2010: Predictability of summer northwest Pacific climate in 11 coupled model hindcasts: Local and remote forcing, *J. Geophys. Res., 115,* D22121, doi:10.1029/2010JD014595

Cooley, D., 2009: Extreme Value Analysis and the Study of Climate Change, (Commentary on Tom Wigley's historical paper "The Climate on the Frequency of Absolute Extreme Events"). *Climate Change*, **97**, 77-83

Deser, C., Wallace, J.M., 1987: El Nino events and their relation to the Southern Oscillation: 1925-1086. *J. Geophys. Res.*, **92**, 14189-14196

Gong, D.Y., Ho, C.H., 2004: Intra-seasonal variability of wintertime temperature over East Asia. *Int. J. Climatol.,* **24**, 131-144

Higgins, R.W., Leetmaa, A., Kousky, V.E., 2001: Relationships between Climate Variability and Winter Temperature Extremes in the United States. *J. Climate*, **15**, 1555-1572

Hu, K., Huang, G., Huang, R., 2011: The impact of tropical Indian Ocean variability on summer surface air temperature in China. *J. Climate*,

Hurrel, J.W., Kushnir, Y., Ottersen, G., Visbeck, M., 2003: An overview of the North Atlantic Oscillation. *The North Atlantic Oscillation: Climate Significance an Environmental Impact, Geophys. Monogr.,* Vol. 134, Amer. Geophys. Union, 1-36

Iwasaki, H., Sato, T., Nii, T., Kimura, F., Nakagawa, K., Kaihotsu, I., Koike, T., 2008: Diurnal Variation of Convective Activity and Precipitable Water around Ulaanbaatar, Mongolia, and the Impact of Soil Moisture on Convective Activity during Nighttime. *Mon. Wea. Rev.,* **136**, 1401-1415

Katz R.W., Brown B.G., 1992: Extreme events in a changing climate: Variability is more important than averages. *Climate Change*, **21**, 3, 289-302

Katz, R.W., 2010: Statistics of extremes in climate changes. *Climate Changes*, **100**, 71-76

Kenyon, J., Hegerl, G.C., 2007: Influence of Modes of Climate Variability on Global Temperature Extremes. *J. Climate*, **21**, 3872-3889

Kiladis, G.N., and Diaz, H.F., 1987: Global climatic anomalies associated with extremes in Southern Oscillation. *J. Climate,* **2**, 1069-1090

Kosaka Y., Nakamura, H., 2006: Structure and dynamics of the summertime Pacific-Japan teleconnection pattern. *Quart. J. Roy. Meteor. Soc.*, **132**, 2009-2030

Kosaka, Y., Nakaumra, H., 2010: Mechanism of Meridional Teleconneciton Observed between a Summer Monsoon System and a Subtropical Anticyclone. Part 1: The Pacific-Japan Pattern. *J. Climate*, **23**, 5085-5108

Liebmann B. and C.A. Smith, 1996: Description of a Complete (Interpolated) Outgoing Longwave Radiation Dataset. *Bulletin of the American Meteorological Society*, **77**, 1275-1277

Mantua, N.J., Hare, S.R., 2002: The Pacific Decadal Oscillation. *J. Oceanogr.* **58**, 35-44

Mantua, N.J., Zhang, Y., Wallace, J.M., Francis, R.C., 1997: A Pacific interdecadal climate oscillation with impacts on salmon production. *Bull. Amer. Meteor. Soc.,* **78**, 1069-1079

Matsumura, S., Xie, S.-P., 1998: Response to Temperature and Precipitation over Japan and the Japan Sea to Variability of Winter Monsoon. *Tenki*, **45**, 781-791

Miyazaki, C., Yasunari, T., 2007: Dominant Interannual and Decadal Variability of Winter Surface Air Temperature over Asia and the Surrounding Oceans. *J. Climate*, **21**, 1371-1386

Munich Re, 2002: Topics, An Annual Review of Natural Catastrophes. Munich Reinsurance Company Publications, Munich, 49 pp

Nakamura, H., 1992: Midwinter suppression of baroclinic wave activity in the Pacific. *J. Atmos. Sci.*, **50**, 2310-2313

Nakamura, H., Wallace, J. M., 1990: Observed changes in baroclinic wave activity during the life cycles of low-frequency circulation anomalies. *J. Atmos. Sci.*, **47**, 1100-1116

Nakamura, H., Izumi, T., Sampe, T., 2002: Interannual and Decadal Modulations Recently Observed in the Pacific Storm Track Activity and East Asian Winter Monsoon. *J. Climate*, **15**, 1855-1874

Ohshima, K.I., Hnashi, S., Hashiya, E., Watanabe, T., 2006: Interannual Variability of Sea Ice Area in the Sea of Okhotsk: Importance of Surface Heat Flux in Fall. *J. Meteor. Soc. Japan*, **84**, 5, 970-919

Onogi, K., Tsutsui, J., Koide, H., Sakamoto, M., Kobayashi, S., Hatsushika, H., Matsumoto, T., Yamazaki, N., Kamahori, H., Takahashi, K., Kadokura, S., Wada, K., Kato, K., Oyama, R., Ose, T., Mannoji, N., Taira, R., 2007: The JRA-25 Reanalysis. *J. Meteor. Soc. Japan*, **85**, 3, 369-432

Ropelewski, C.F., Jones, P.D., 1987: An Extension of the Tahiti-Darwin Southern Oscillation Index. Mon. Wea. Rev., **115**, 2161-2165

Scaife, A.A., Folland, C.K., Alexander, L.V., Moberg, A., Knight, J.R., 2007: European Climate Extremes and the North Atlantic Oscillation. *J. Climate*, **21**, 72-83

Thompson, D.W.J., Wallace, J.M., 1999: Annular Modes in the Extratropical Circulation. Part 1: Month-to-Month Variability. *J. Climate*, **13**, 1000-1016

Thompson, D.W.J., Wallace, J.M., Hegerl, G.C., 1999: Annular Modes in the Extratropical Circulation. Part 2: Trends. *J. Climate*, **13**, 1018-1036

Tomita, T., Yasunari, T., 1996: Role of the northeast winter monsoon on the biennial oscillation of the ENSO/Monsoon system. *J. Meteor. Soc. Japan*, **74**, 399-413

Wakabayashi, A., Kawamura, R., 2004: Extraction of Major Teleconnection Patterns Possibly Associated with the Anomalous Summer Climate in Japan. *J. Meteor. Soc. Japan*, **82**, 1577-1588

Wang, B., Wu, Z., Chang, C.-P., Liu, J., Li, J., Zhou, T., 2009: Another Look at Interannual-to-Interdecadal Variations of the East Asia Winter Monsoon: The Northern and Southern Temperature Modes. *J. Climate*, **23**, 1495-1512

Webster, P.J., 2006: The Elementary Monsoon. The Asian Monsoon, Wang, B. Ed, Praxis, 3-32

Wettesen, J., Mearns, L.O., 2002: The influence of the North Atlantic – Arctic Oscillation on mean, variance, and extremes of temperature in the northeastern United States and Canada. *J. Climate,* **15**, 3586-3600

Wu, B., Wang, J., 2002: Winter Arctic Oscillation, Siberian High and Eats Asia Winter Monsoon. Geophysical Research Letters, Vol.29, No.19, 1897

Xie, P., Arkin, P.A., 1997: Global precipitation: A 17-year monthly analysis based on gauge observations, sattellite estimates, and numerical model outputs. *Bull. Amer. Meteor. Soc*., **78**, 2539-2558

Xie, S.-P., Noguchi, H., Matsumura, S., 1999: A Hemispheric-Scale Quasi-Decadal Oscillation and Its Signature in Northern Japan. *J. Meteor. Soc. Japan*, **77**, 573-582

Xie, S.-P., Hu, K., Hafner, J., Tokinaga, H., Du, Y., Huang, G., Sampe, T., 2009: Indian Ocean Capacitor Effect on Indo-Western Pacific Climate during the Summer following El Nino. *J. Climate*, **22**, 730-747

Xie, S.-P., Du, Y., Huang, G., Zheng, X.-T., Tokinaga, H., Hu, K., Liu, Q., 2010: Decadal shift in El Nino Influences on Indo-Western Pacific and East Asian Climate in the 1970s. *J. Climate*, **23**, 3352-3368

Yasunaka, S., Hanawa, K., 2006: Interannual Summer Temperature Variations over Japan and Their Relation to Large-Scale Atmospheric Circulation Field. *J. Meteor. Soc. Japan*, **84**, 641-652

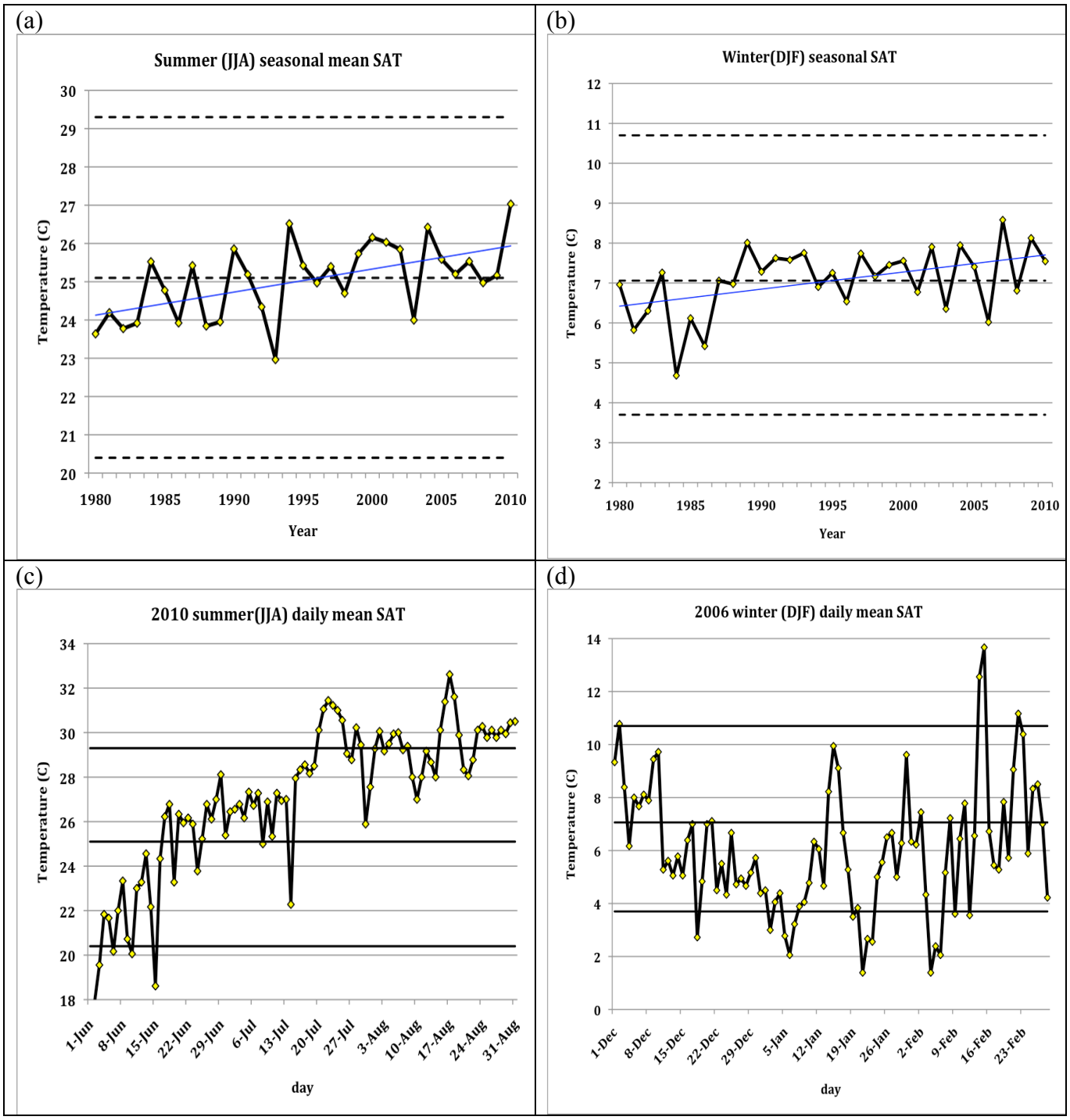

Figure 1
(a) Summer (JJA) and (b) winter (DJF) seasonal mean time series of SAT at Tokyo station for 1980-2010. The blue line is the trend. The daily mean time series of SAT for (c) summer 2010 and (d) winter 2006 are also shown. The dashed lines in (a, b) and solid lines in (c, d) represent the climatological mean 10^{th} and 90^{th} percentiles, and mean of the SAT distribution.

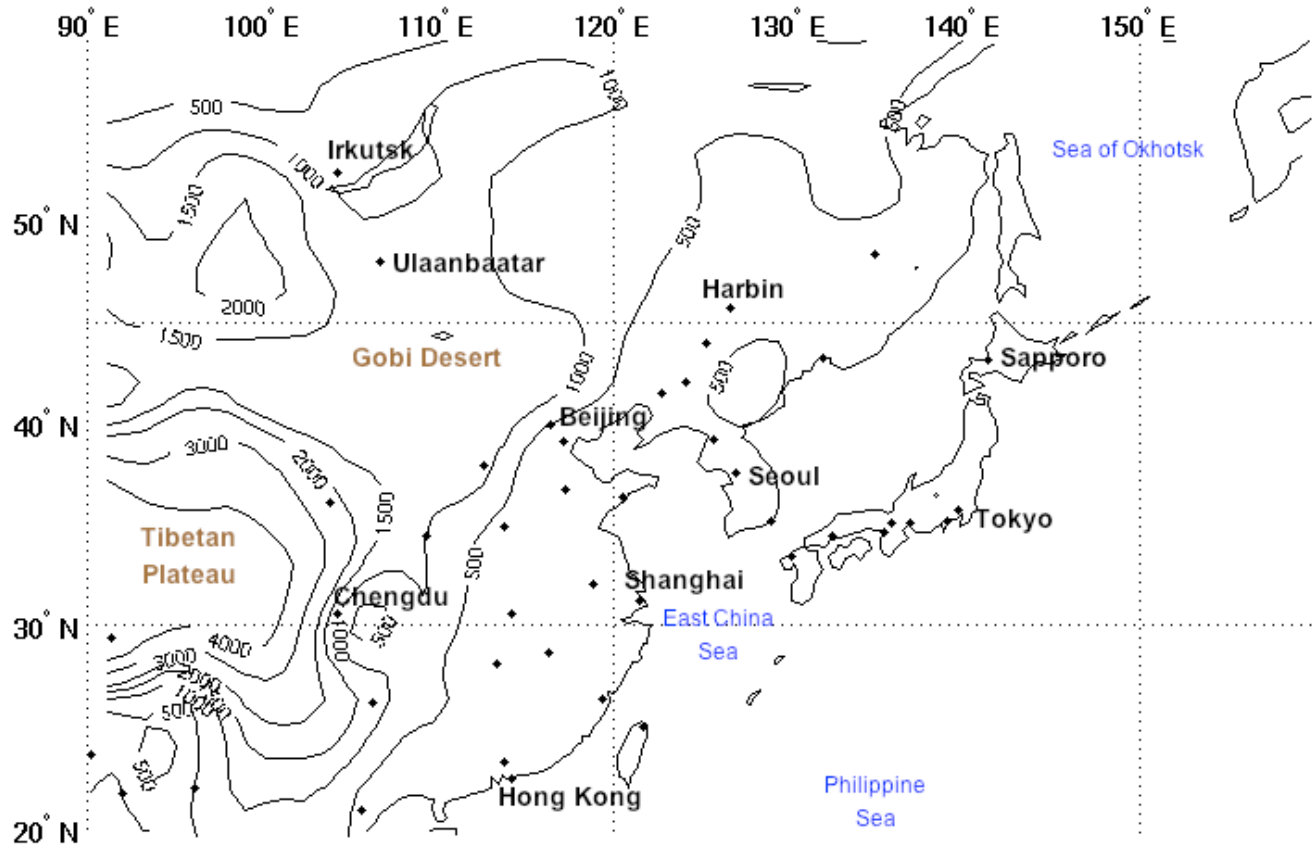

Figure 2
Surface geometric height (contour, m) over East Asia that is used in JRA-25 reanalysis model.

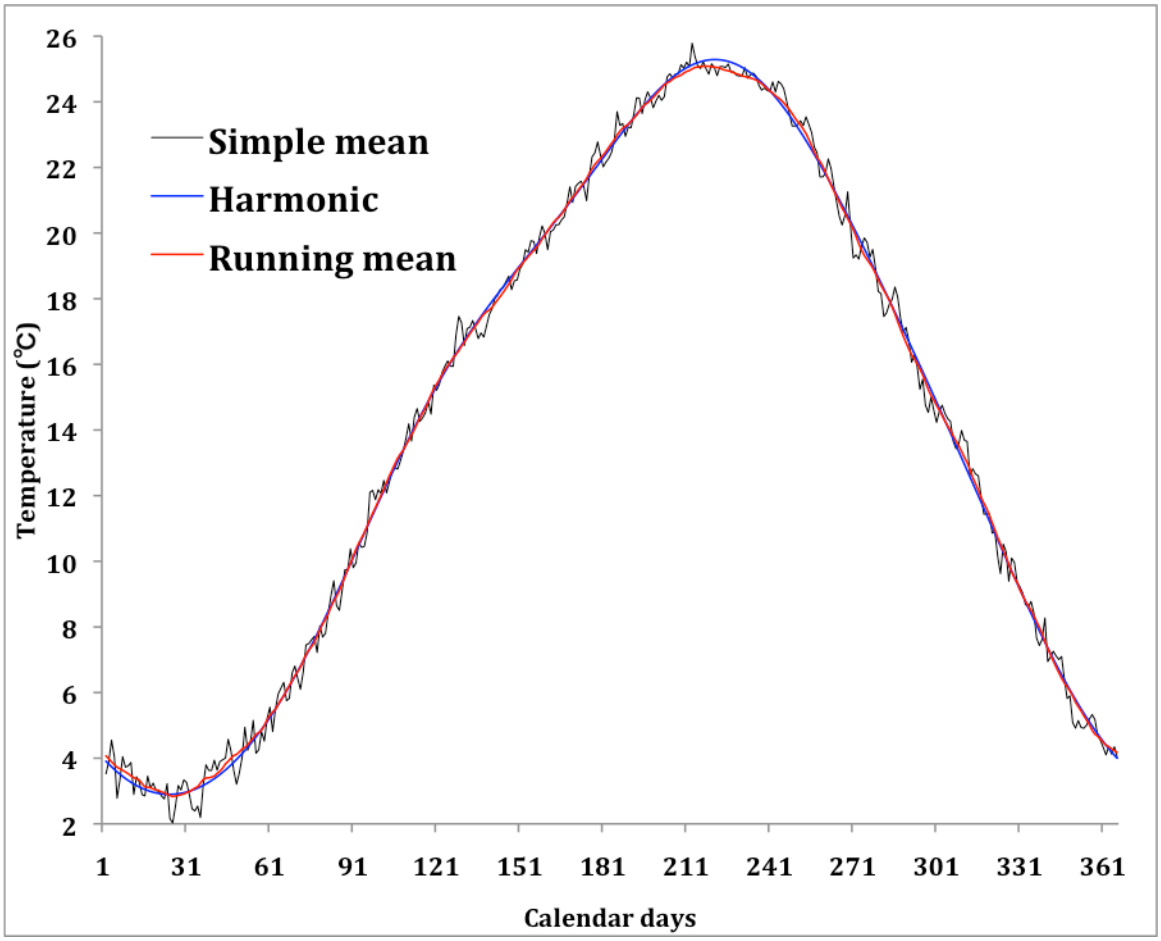

Figure 3
Annual cycle of simple calendar day mean (black) of SAT in Tokyo for 1979-2009. The smoothed cycle by Harmonic smoothing and by 21-day running mean are shown as a blue and red line, respectively.

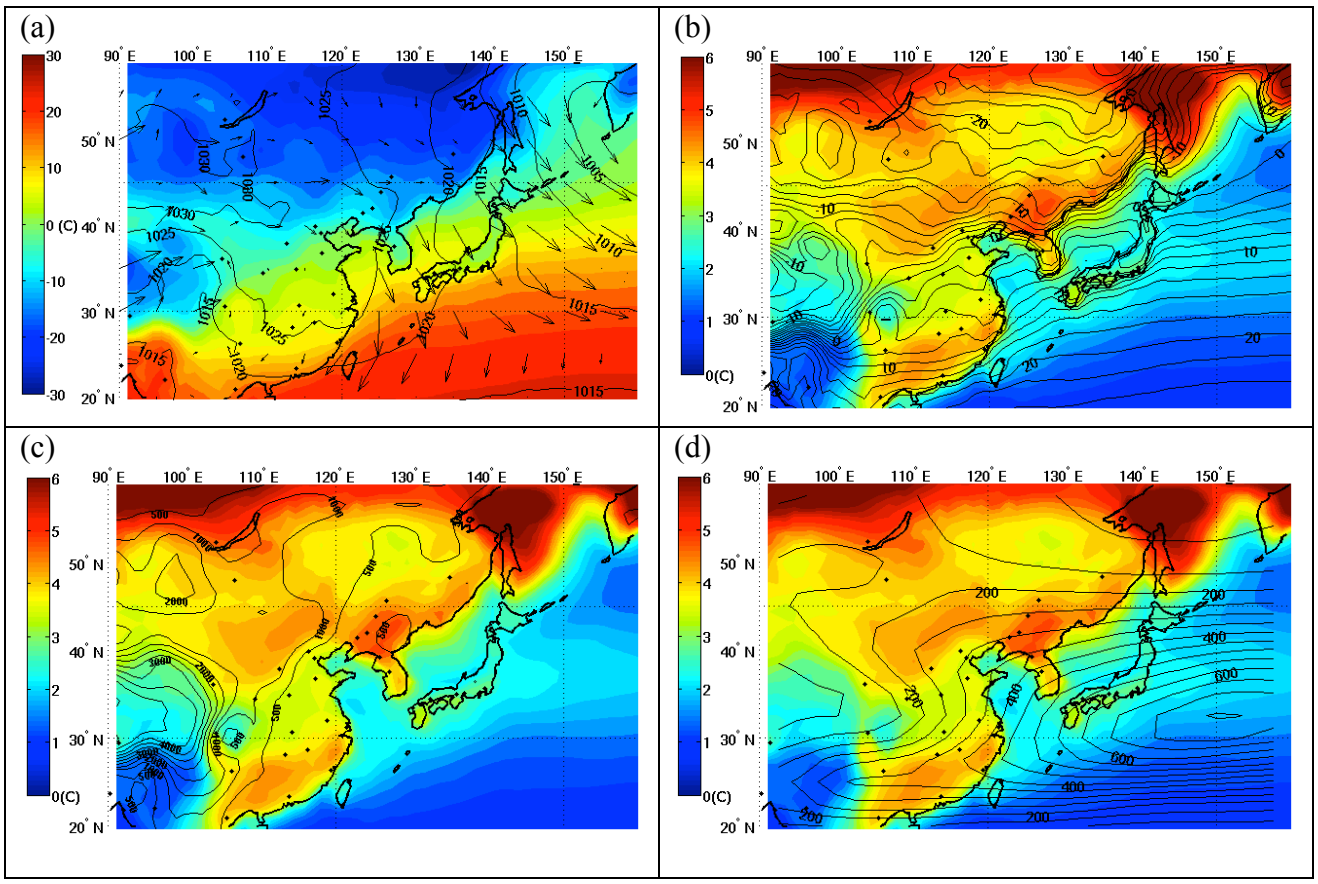

Figure 4
Winter (DJF) climatology. (a) SAT (color, °C), MSLP (contour, hPa), and surface wind (vector). Subseasonal SAT standard deviation (color, °C) with (b) climatology of SAT (contour, °C), (c) orography (contour, m), and (d) eddy kinetic energy at the 500-hPa level (contour, m^2/s^2).

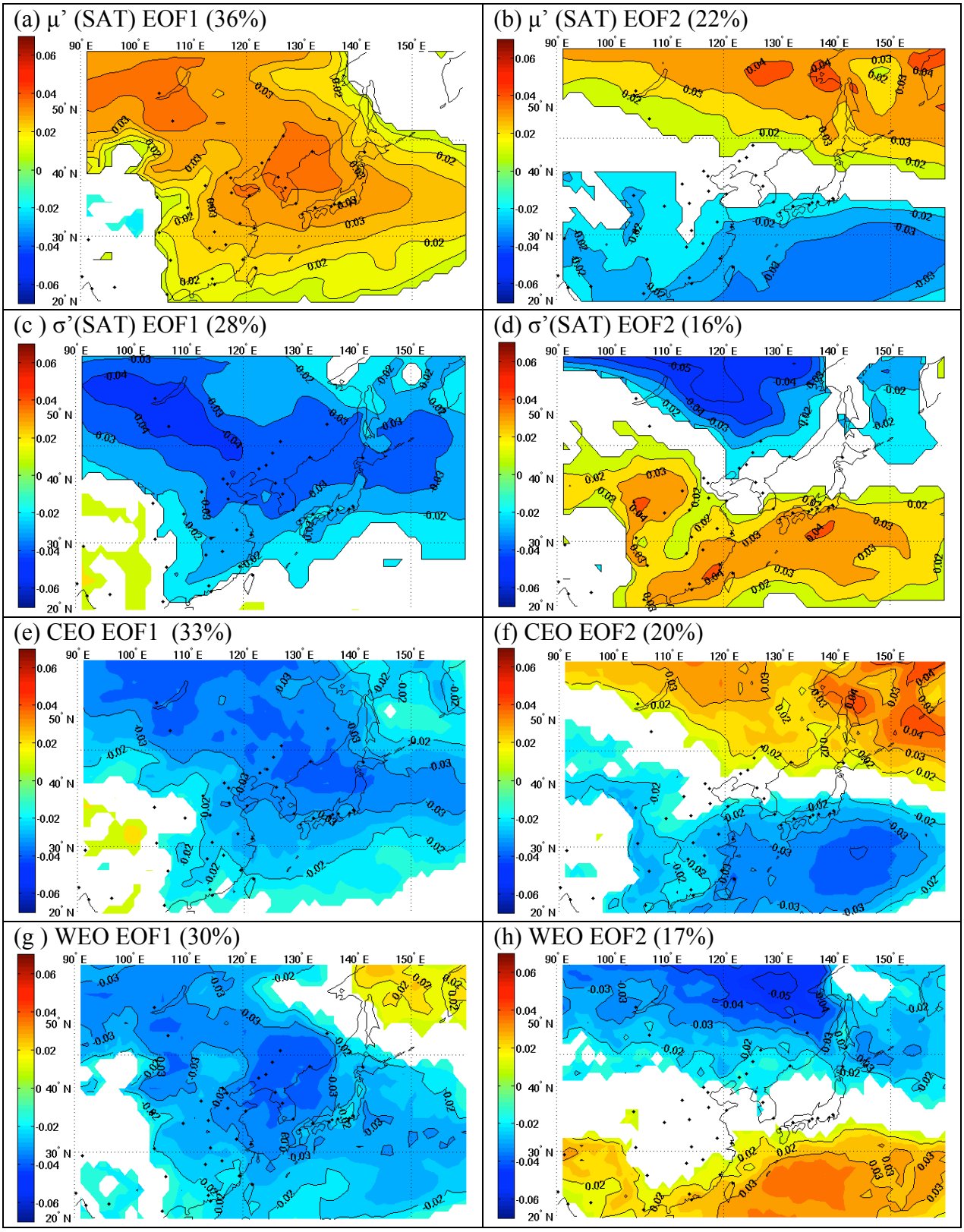

Figure 5
Spatial distribution of the first (left column) and second (right column) EOF on winter (a,b) seasonal mean SAT, (c,d) subseasonal SAT deviation, (e,f) seasonal frequency of Cold Extreme Occurrences(CEO), and (g,h) that of Warm Extreme Occurrences (WEO). The percentages are explained variance to the total variance. Contour intervals are arbitrary in each figure.

Table 1		μ (SAT)		σ (SAT)		Cold extreme		Warm extreme	
	PCs %	PC1 36%	PC2 22%	PC1 28%	PC2 16%	PC1 33%	PC2 20%	PC1 30%	PC2 17%
μ (SAT)	PC1								
	PC2								
σ (SAT)	PC1	0.33	(e) *0.55						
	PC2	(g) -0.26	0						
Cold extreme	PC1	* 0.9	0.3	*0.62	-0.1				
	PC2	0.35	*-0.84	-0.44	-0.34				
Warm extreme	PC1	*-0.83	0.4	0.12	0.21	*-0.55	*-0.58		
	PC2	-0.3	*-0.78	-0.26	0.4	-0.39	0.4		
Large-scale index	AO	(a) *0.58	(c) 0.36	(f) *0.5	-0.07	*0.67	-0.16	-0.33	-0.36
	MOI	(b)*-0.73	0.22	-0.05	(h) 0.38	*-0.5	*-0.52	*0.69	0.17
	SOI	0.16	(d) -0.35	-0.35	-0.11	0.02	*0.5	-0.24	0.03

Table 1
Correlation coefficients between PCs in winter seasonal mean SAT, subseasonal SAT deviation, cold and warm extreme occurrences, and large-scale circulation indices. (*) indicates a correlation coefficient that is statistically significant at the 99% level.

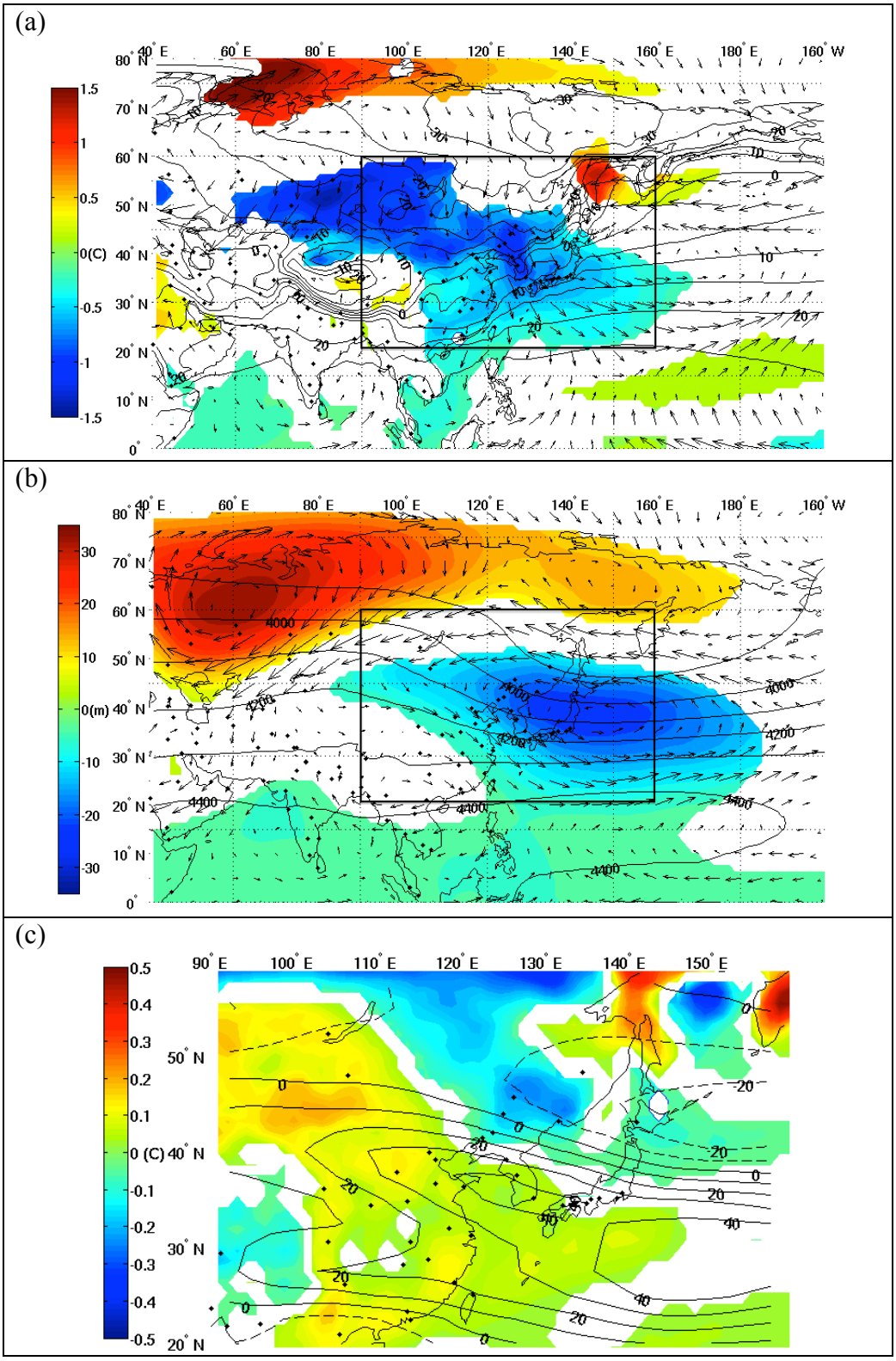

Figure 6

Regression of circulation anomalies with MOI. (a) SAT (color, °C) and 925-hPa wind (vector). (b) 500-hPa geopotential height (color, m) and 500-hPa wind (vector). (c) subseasonal SAT deviation (color, °C) and 500-hPa eddy kinetic energy (contour, m^2/s^2). Climatological SAT and 500h-Pa geopotetial height are plotted as contours in (a) and (b), respectively. Color shading in (a) and (b) is only applied to values that are statistically significant at the 90% level. The blocks in (a) and (b) represent the same domain as in (c).

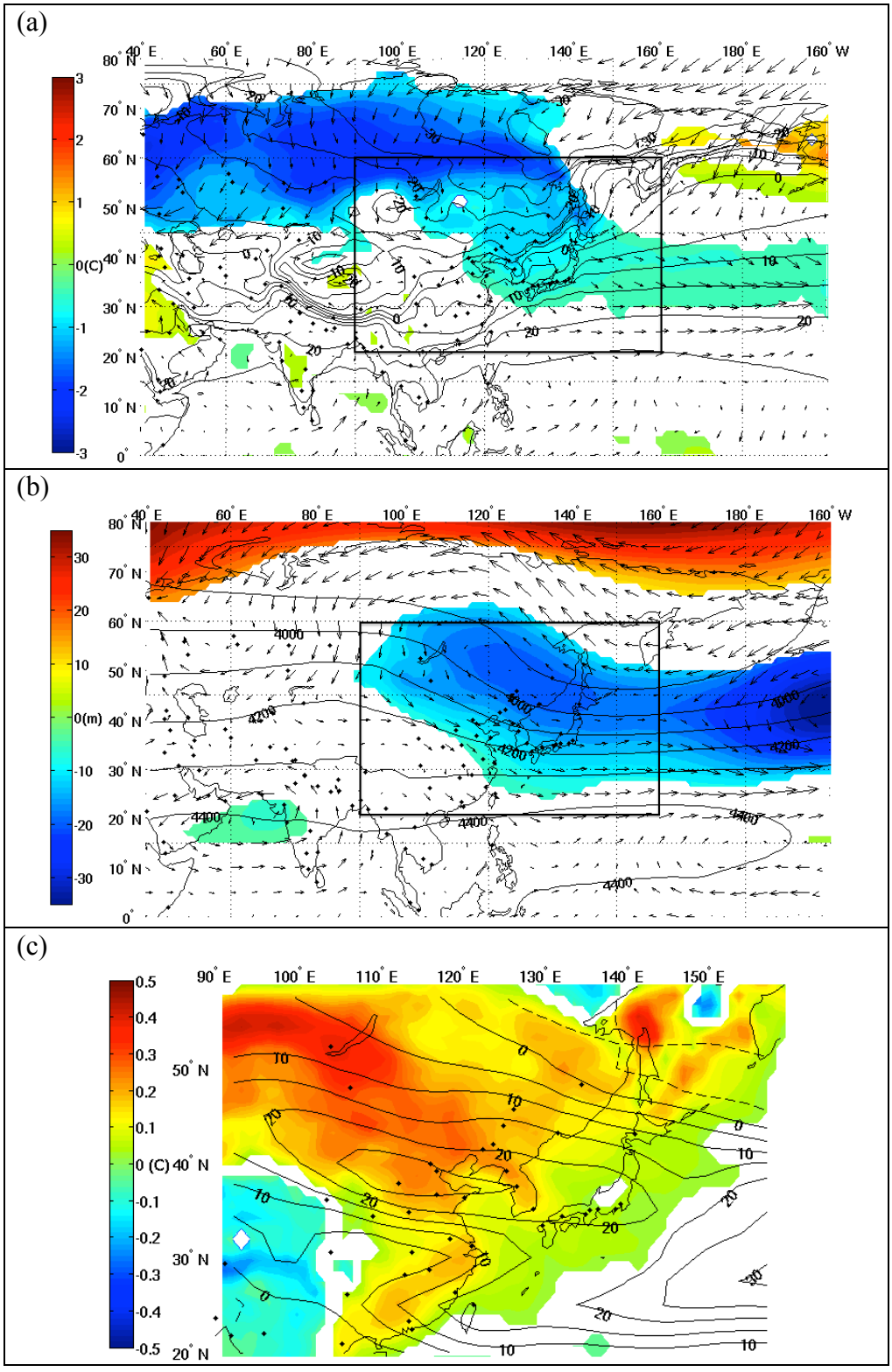

Figure 7
As in Fig. 6 but for regressions with the negative phase of the AO.

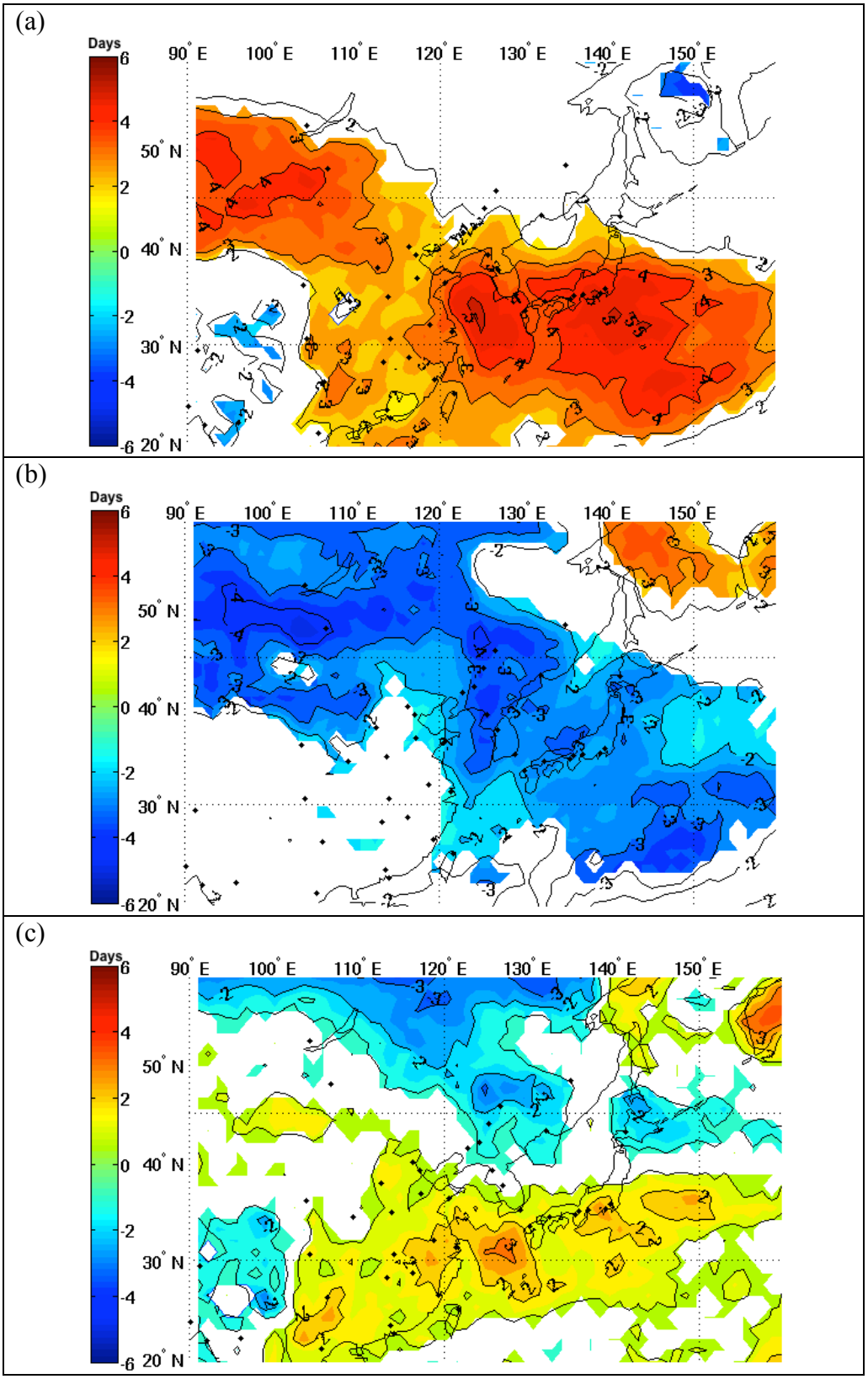

Figure 8
Regression of extreme occurrences with MOI. (a) Cold and (b) warm extreme occurrences (color, days). Color shading is the value that is statistically significant at the 90% level. (c) Spatial distributions of asymmetry of regression coefficients between them.

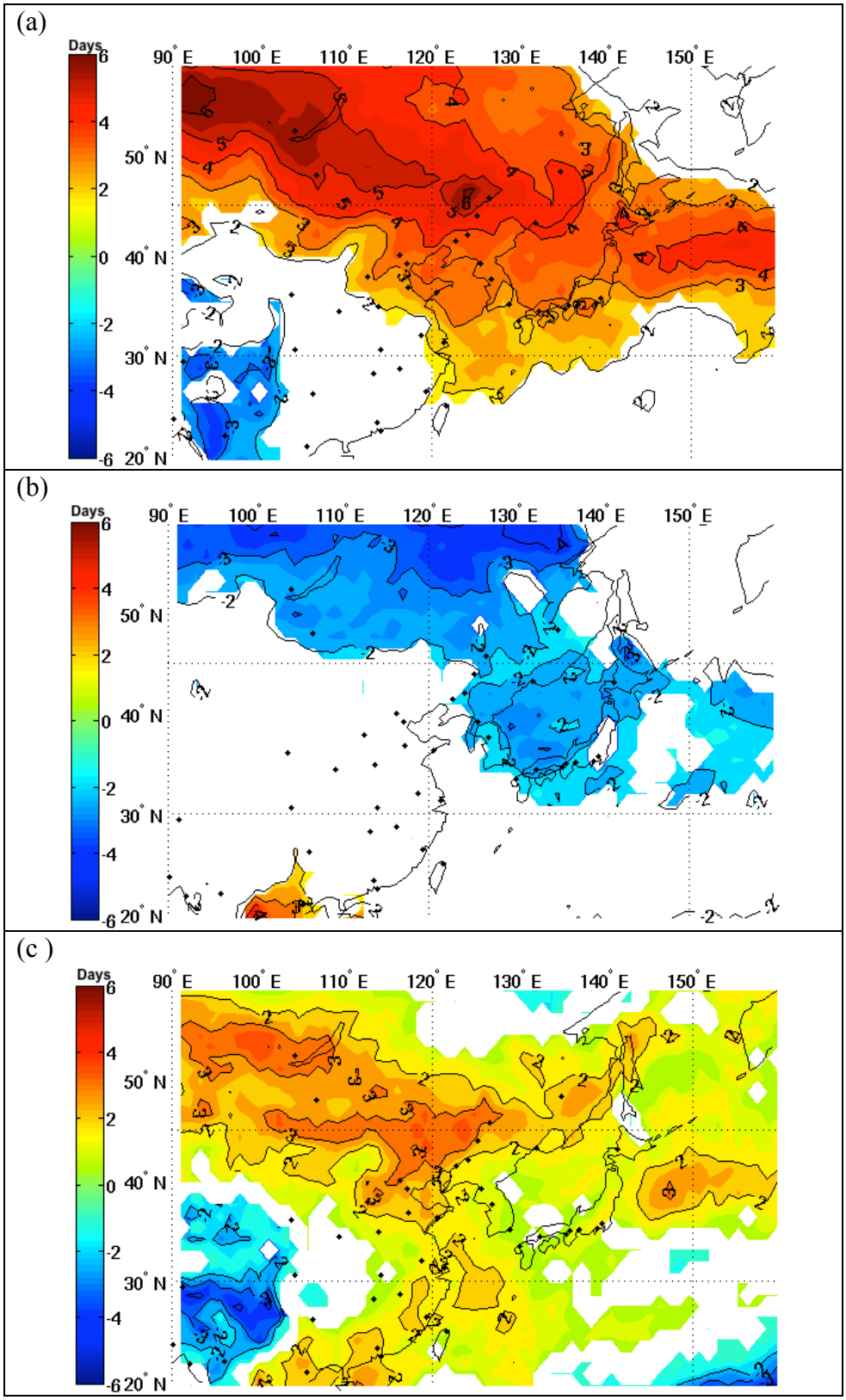

Figure 9
As in Fig. 8 but for regressions with the negative phase of the AO.

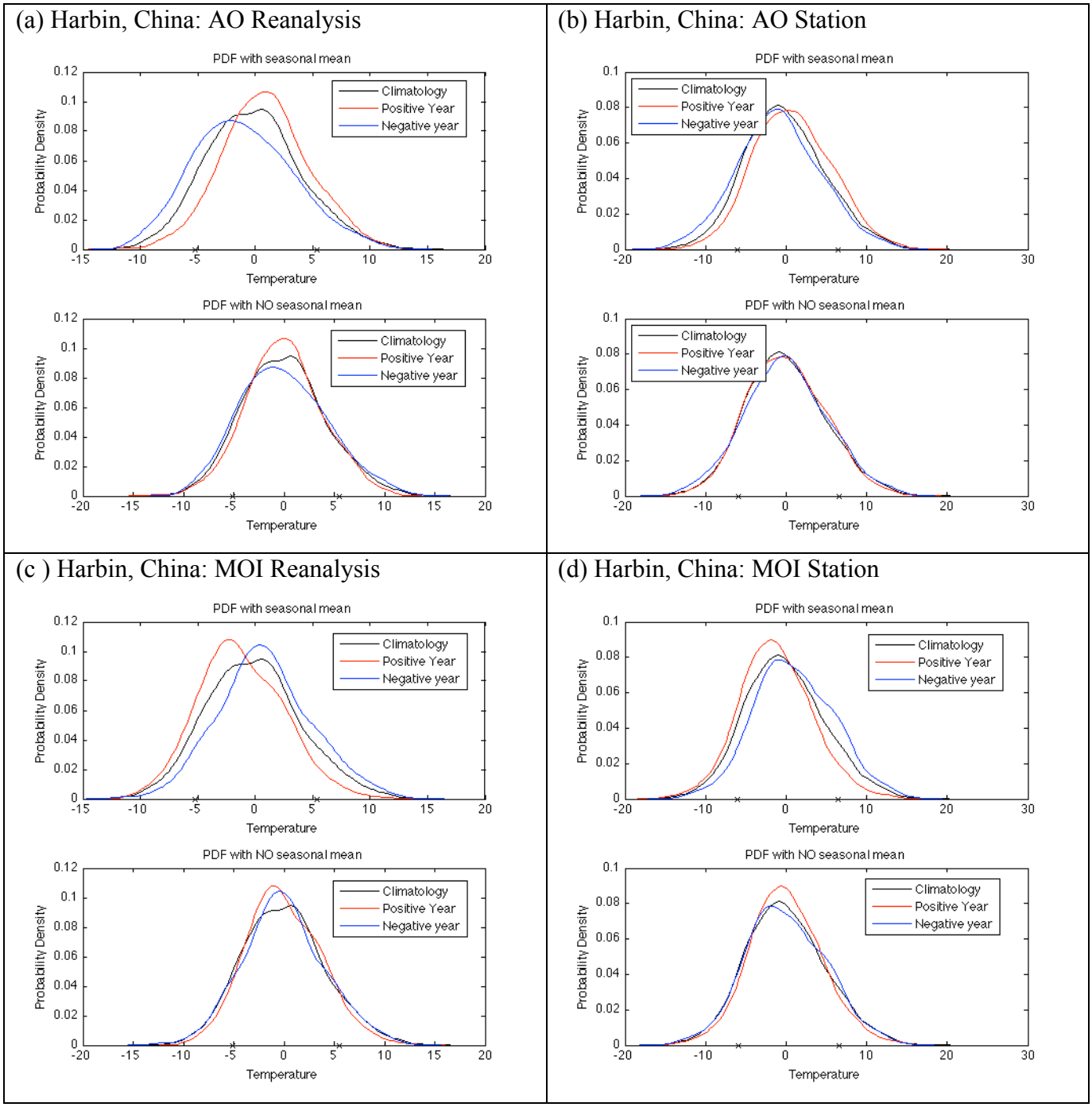

Figure 10
Smoothed histograms of daily mean SAT anomalies at Harbin, China, based on phase of the AO (a,b) and MOI (c,d), using the reanalysis data (a,c) and station data (b,d). Each composite consists of distribution in climatology (black), positive phase (red), and negative phase (blue). The upper plots in each figure are based on the raw anomalies and the lower plots are based on the anomalies with seasonal mean removed. The 10^{th} and 90^{th} percentiles of climatological distribution are shown as 'x' in each plot.

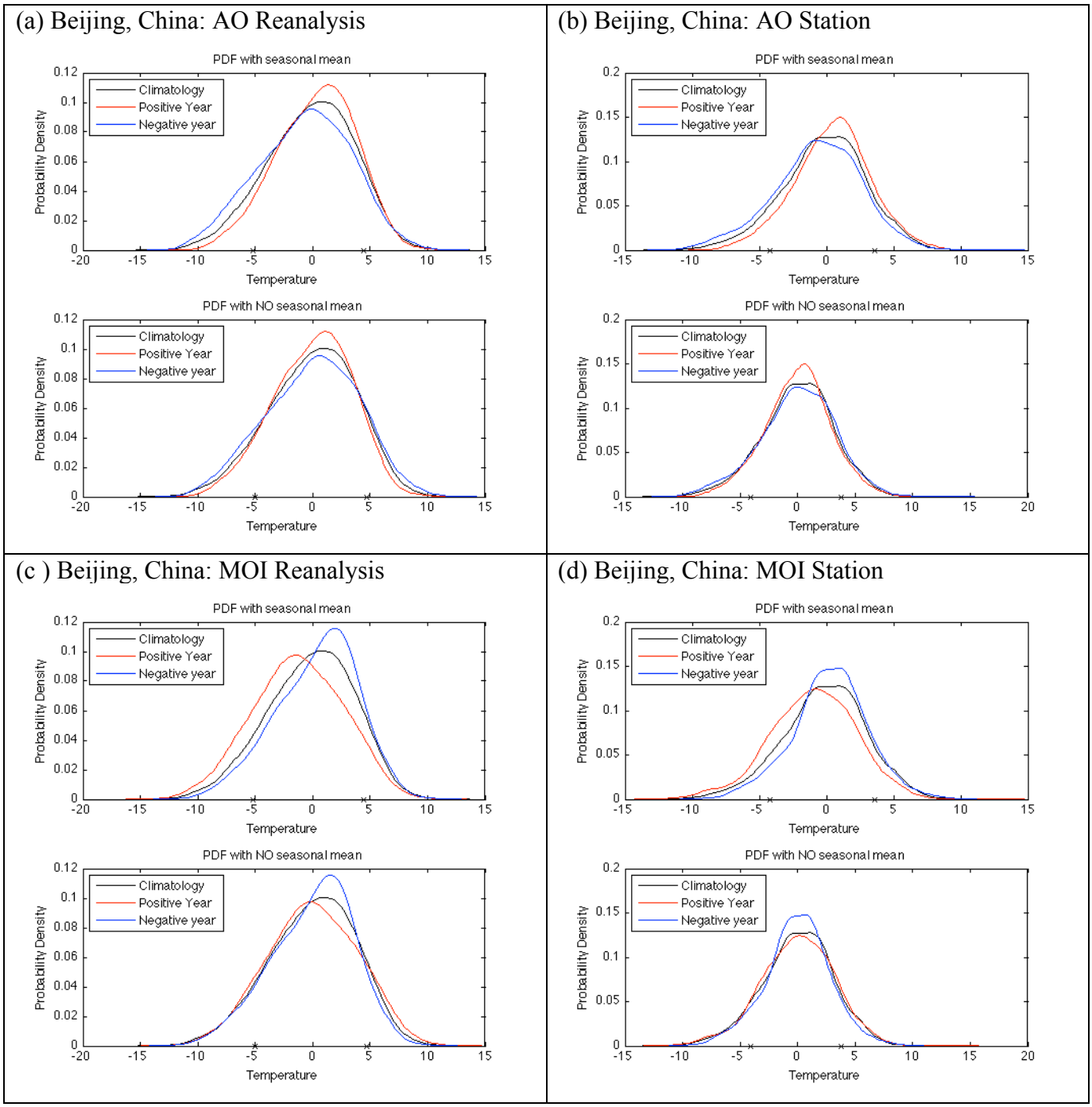

Figure 11
As in Fig. 10 but for Beijing, China.

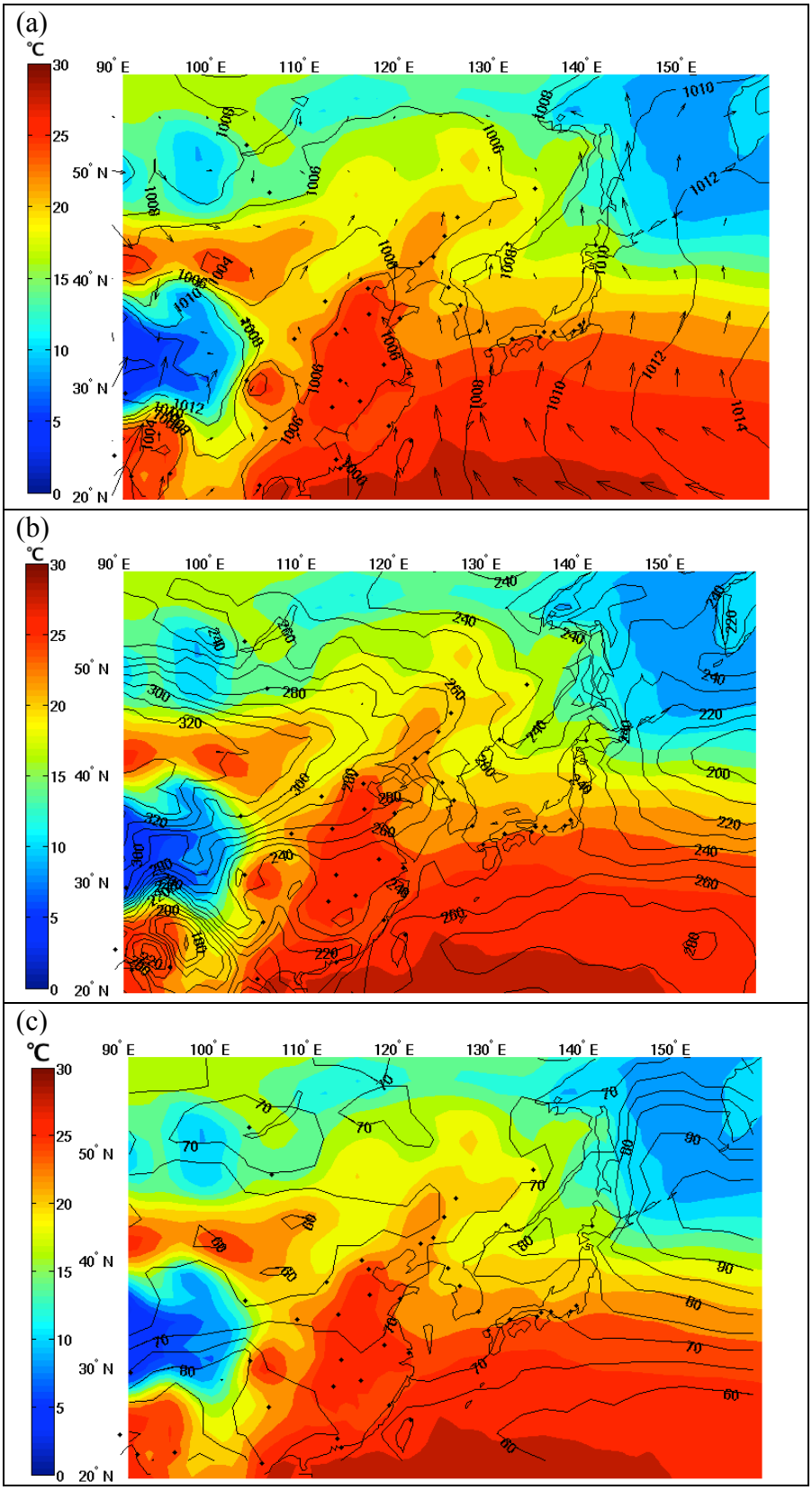

Figure 12
Summer (JJA) climatology of seasonal mean SAT (color, °C) with (a) MSLP (contour, hPa) and surface wind (vector), (b) Downward solar radiation flux (contour, W/m^2), and (c) cloud amount (contour, %).

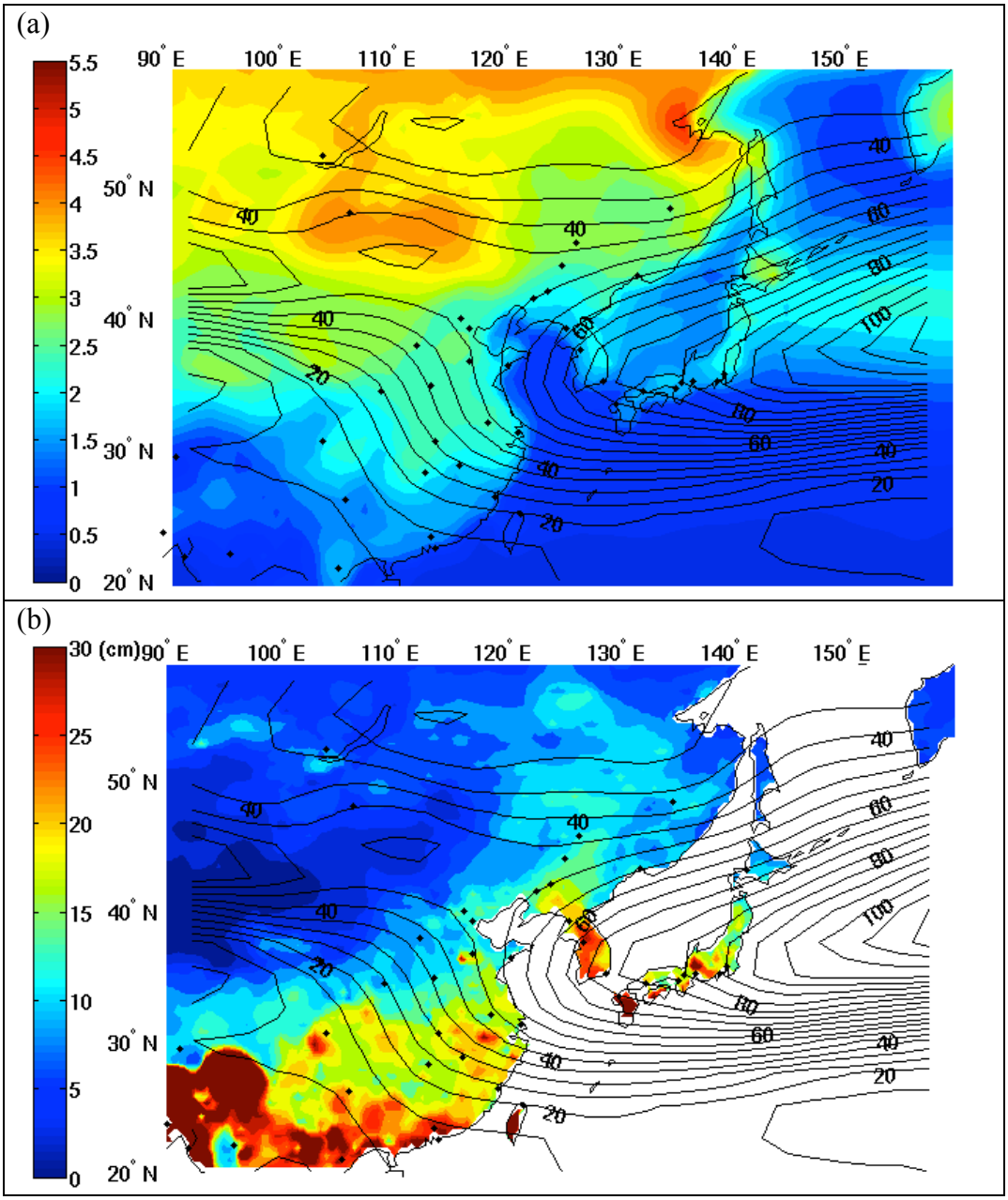

Figure 13
Summer (JJA) climatology of subseasonal SAT variability. (a) Standard deviation of subseasonal SAT (color, °C) and 500-hPa eddy kinetic energy (contour, m^2/s^2). (d) Precipitation (color, cm) and eddy kinetic energy at the 500-hPa level (contour, m^2/s^2).

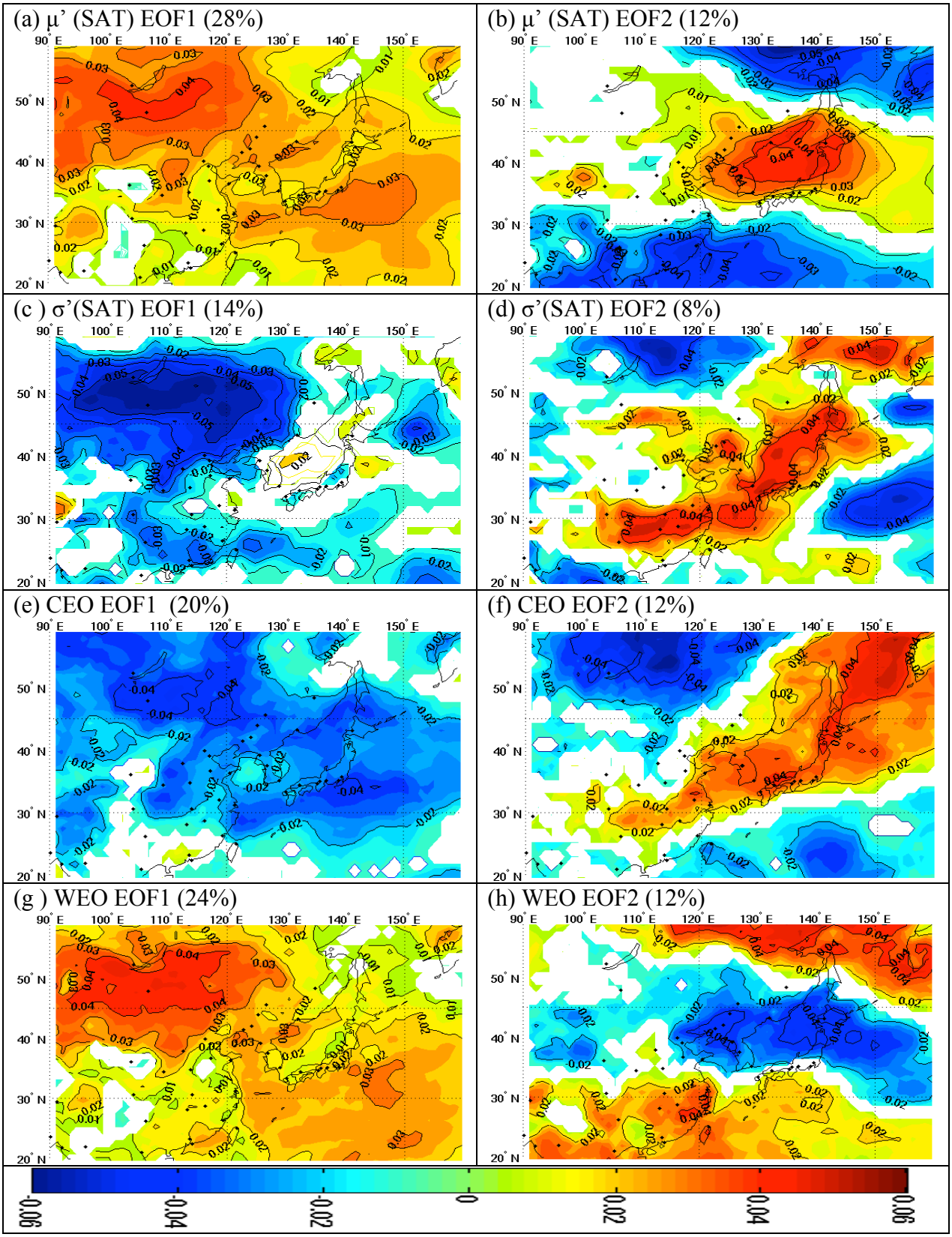

Figure 14
Spatial pattern of the first (left column) and second (right column) EOF on summer (a,b) seasonal mean SAT, (c,d)subseasonal SAT deviation, (e,f) seasonal mean frequency of CEO, and (g,h) that of WEO. The percentages are explained variance to the total variance. Contour intervals are arbitrary in each figure.

Table		μ(SAT)		σ(SAT)		Cold extreme		Warm extreme	
	PCs %	PC1 28%	PC2 12%	PC1 14%	PC2 8%	PC1 20%	PC2 12%	PC1 24%	PC2 12%
μ(SAT)	PC1								
	PC2								
σ(SAT)	PC1	(c) -0.43	-0.15						
	PC2	-0.01	0.05						
Cold extreme	PC1	(e) *0.93	0.04	-0.18	-0.08				
	PC2	0.06	-0.3	0.14	(i) *0.53				
Warm extreme	PC1	(f) *0.96	-0.01	(h) *-0.54	0.05	*0.82	0.17		
	PC2	0.04	(g) *-0.9	0.18	-0.23	0.06	0.13		
Large-scale index	SOI(NDJF)	(a) 0.41	0.36	(d) -0.32	0.05	0.37	-0.1	0.37	-0.33
	PJ	0.14	(b) *0.67	-0.13	-0.06	0.19	-0.14	0.09	*-0.56

Table 2
Correlation coefficients between PCs in summer seasonal mean SAT, subseasonal SAT deviation, cold and warm extreme occurrences, and large-scale circulation indices. (*) indicates a correlation coefficient that is statistically significant at the 99% level.

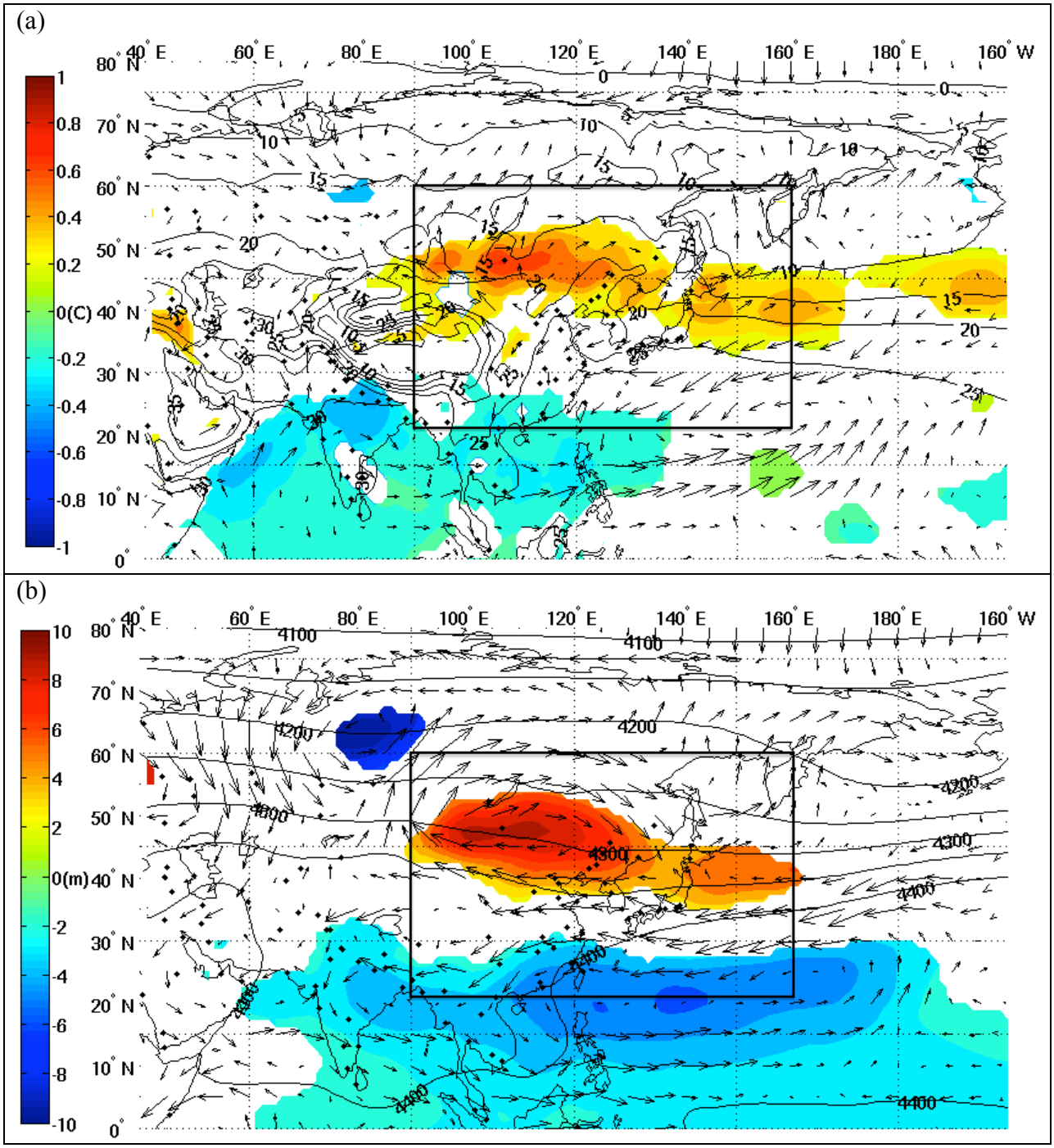

Figure 15
Regression of circulation anomalies with the preceding winter SOI. (a) SAT (color, °C) and 925 -hPa wind (vector). (b) 500-hPa geopotential height (color, m) and 500-hPa wind (vector). Climatological SAT and 500-hPa geopotetial height are plotted as contours in (a) and (b), respectively. Color shading is only applied to values that are statistically significant at the 90% level. The blocks represent the same domain as the original East Asia domain.

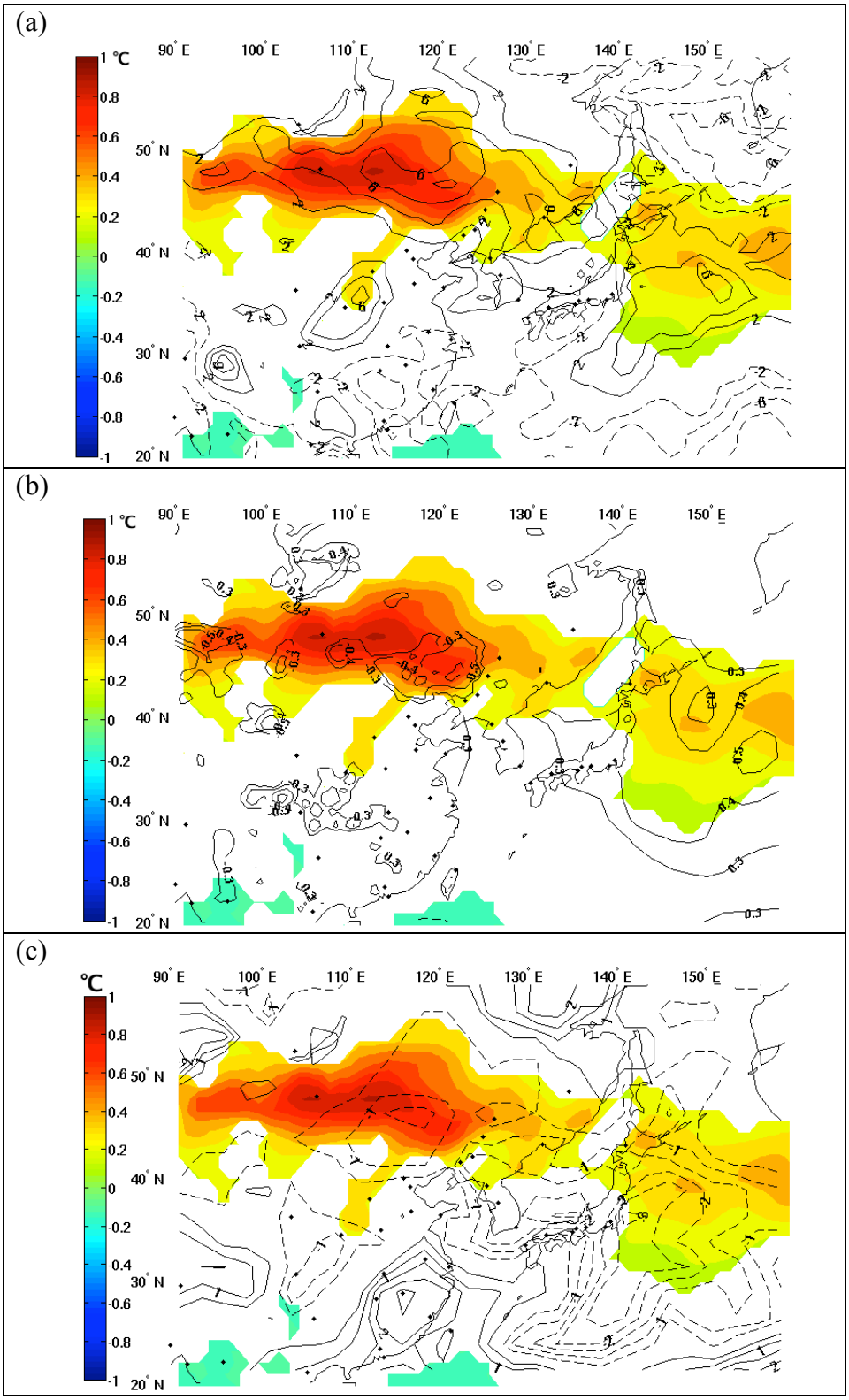

Figure 16

Regression and correlation coefficients of summer (JJA) seasonal mean SAT with the preceding winter SOI. Regression of JJA seasonal mean SAT (color, °C) with (a) Downward solar radiation flux (contour, W/m^2), (b) Correlation of precipitation (contour over land) and of SST (contour over ocean), and (c) Regression of cloud amount (contour, %). Color shading is only applied to values that are statistically significant at the 90% level.

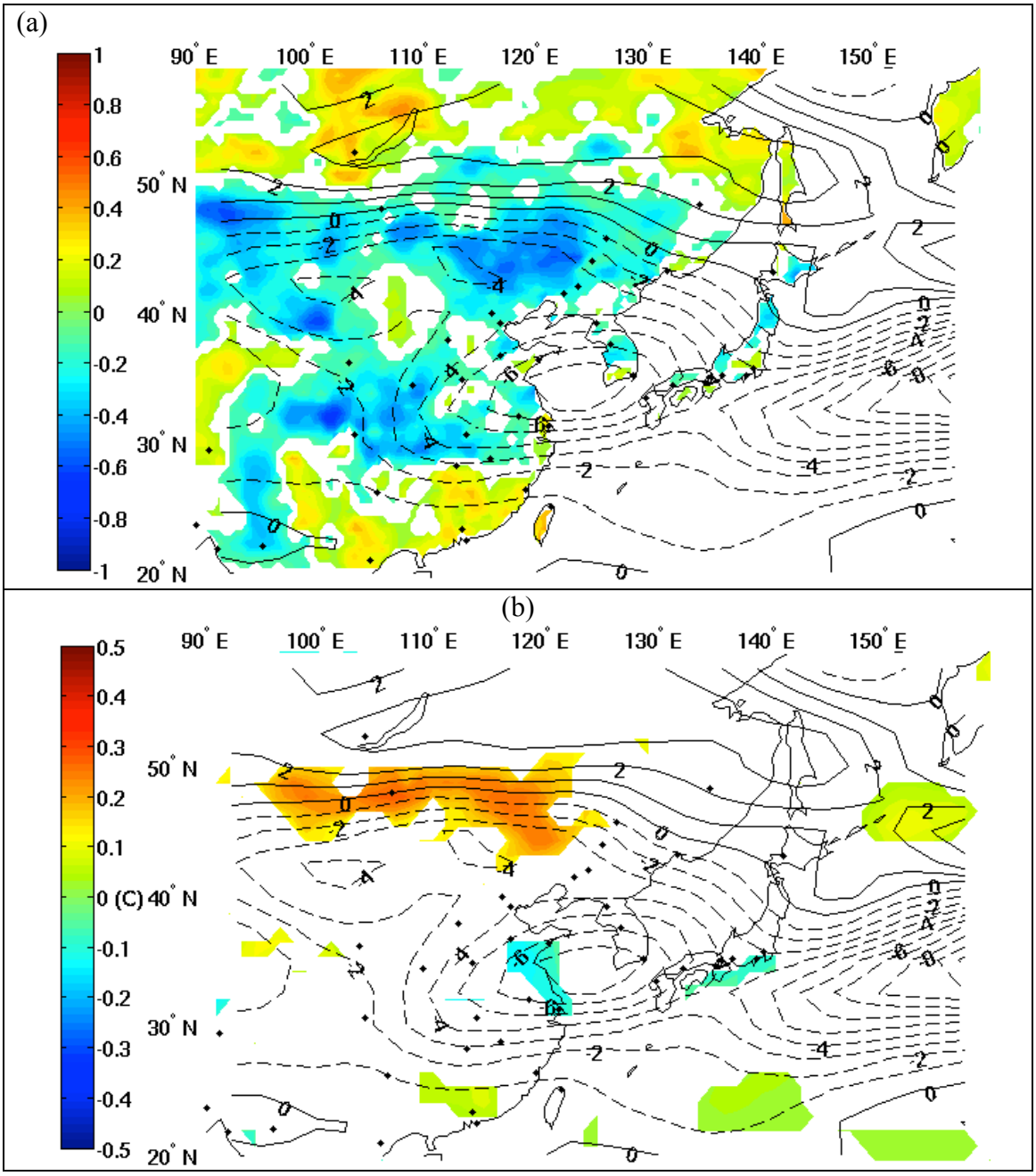

Figure 17

Regression and correlation coefficients of standard deviation of summer (JJA) subseasonal SAT with the preceding winter SOI. (a) Regression of 500-hPa eddy kinetic energy (contour, m^2/s^2) and correlation of precipitation (color). (b) Regression of standard deviation of subseasonal SAT (color, °C) and 500-hPa eddy kinetic energy (contour, m^2/s^2). Color shading in (b) is only applied to values that are statistically significant at the 90% level.

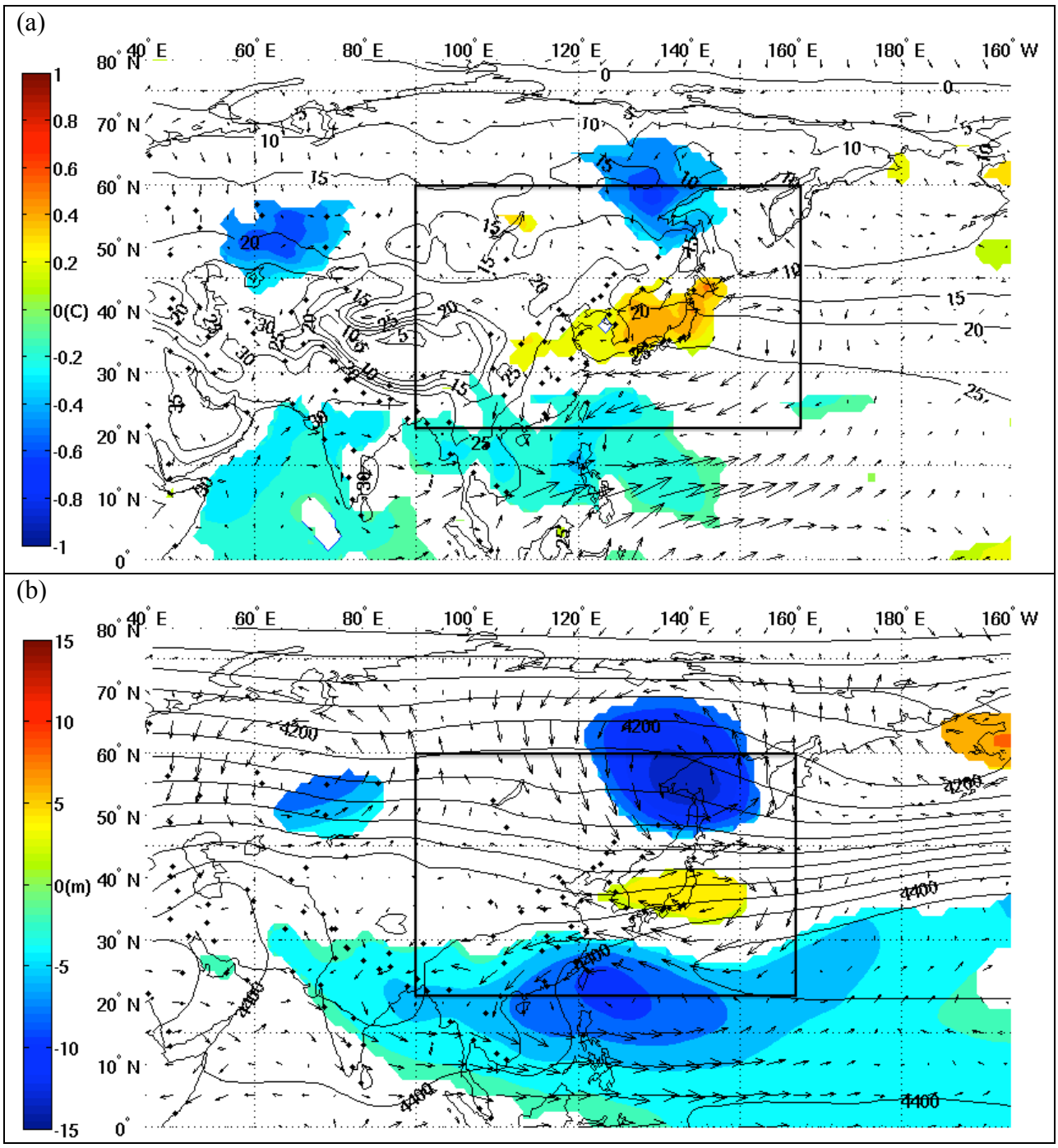

Figure 18
As in Fig. 15 but for the PJ.

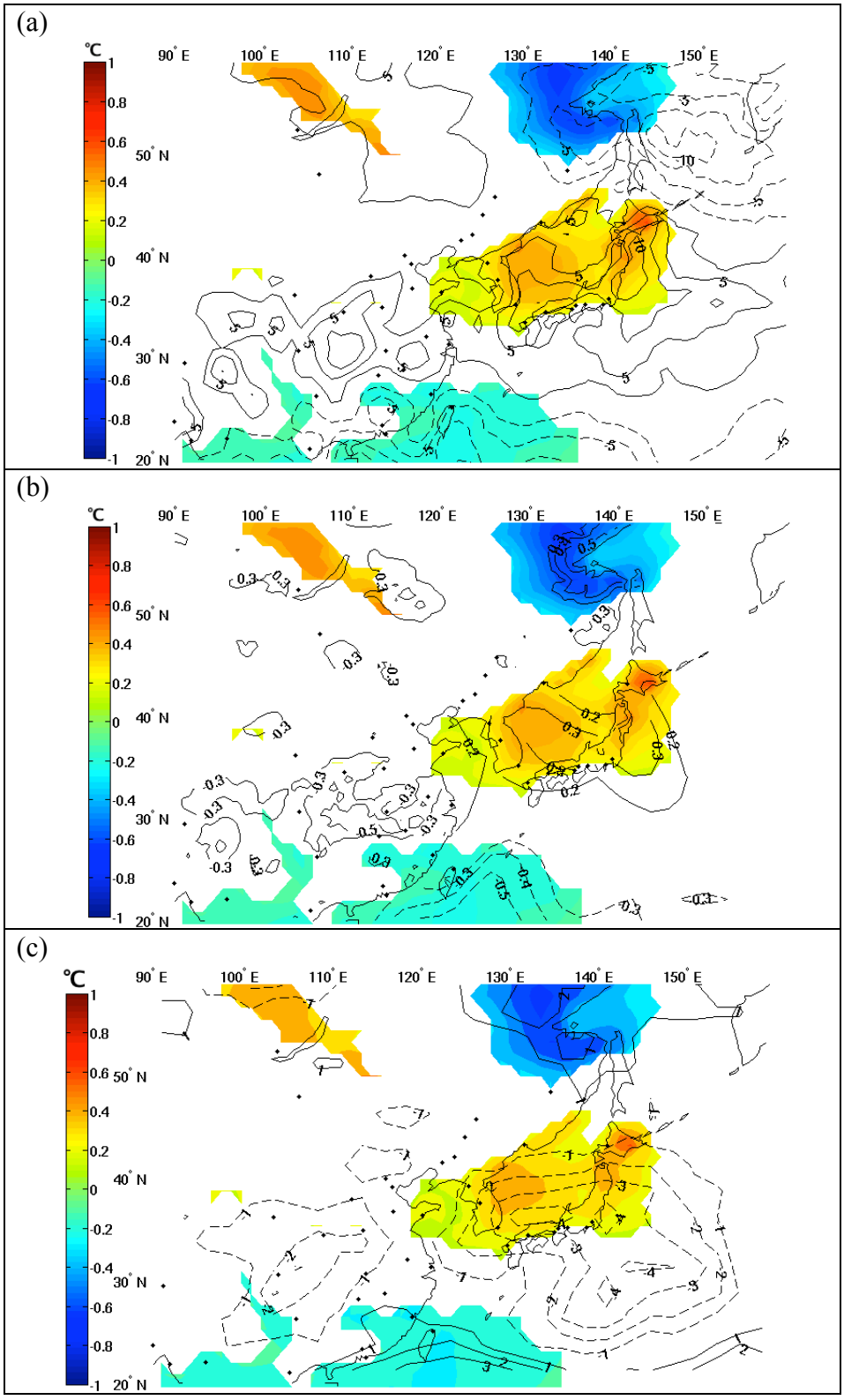

Figure 19
As in Fig. 16 but for the PJ.

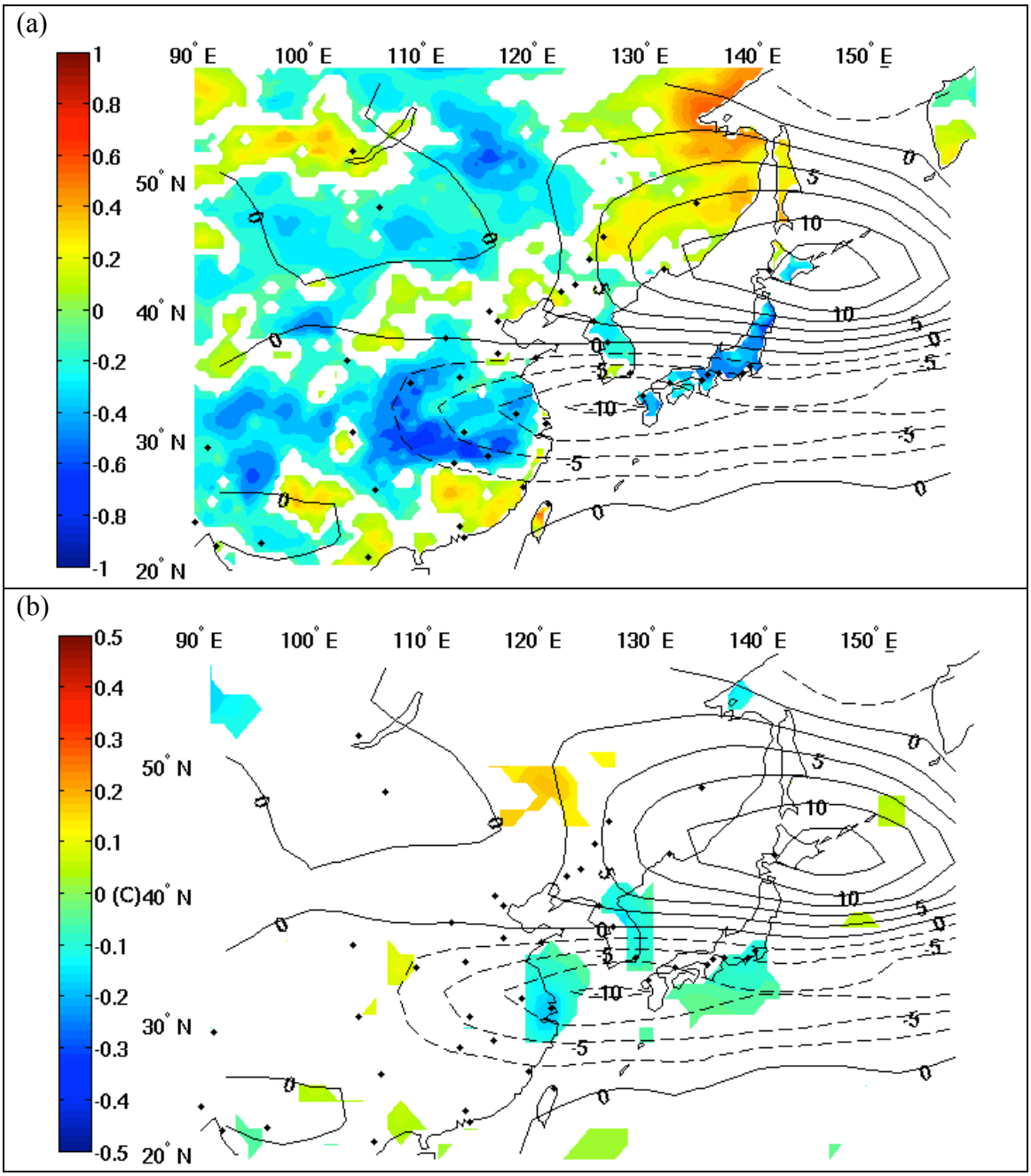

Figure 20
As in Fig. 17 but for the PJ.

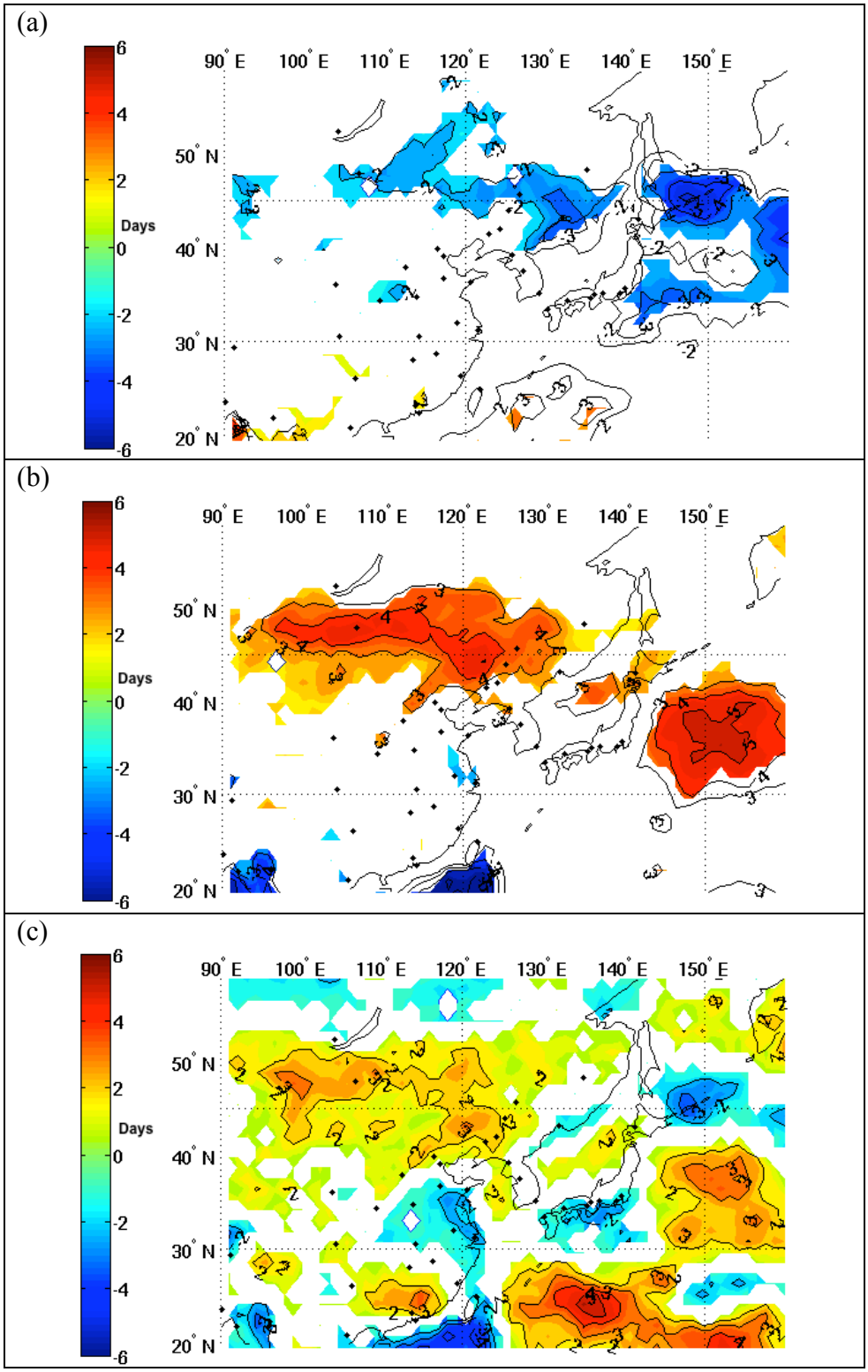

Figure 21
Regression of extreme occurrences with the preceding winter SOI. (a) Cold and (b) warm extreme occurrences (color, days). Color shading is the value that is statistically significant at the 90% level. (c) Spatial distributions of asymmetry of regression coefficients between them.

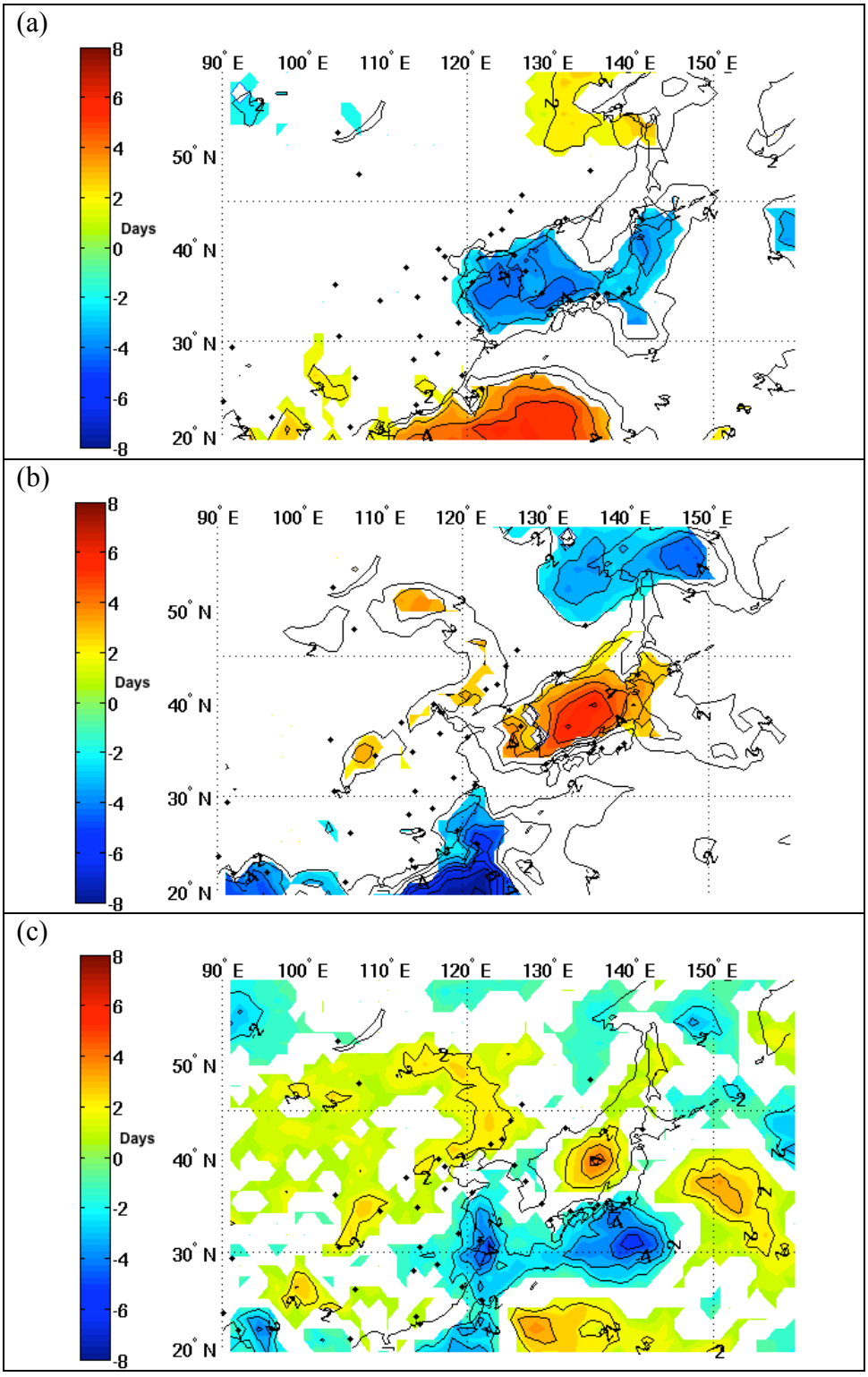

Figure 22
As in Fig. 21 but for regressions of the PJ.

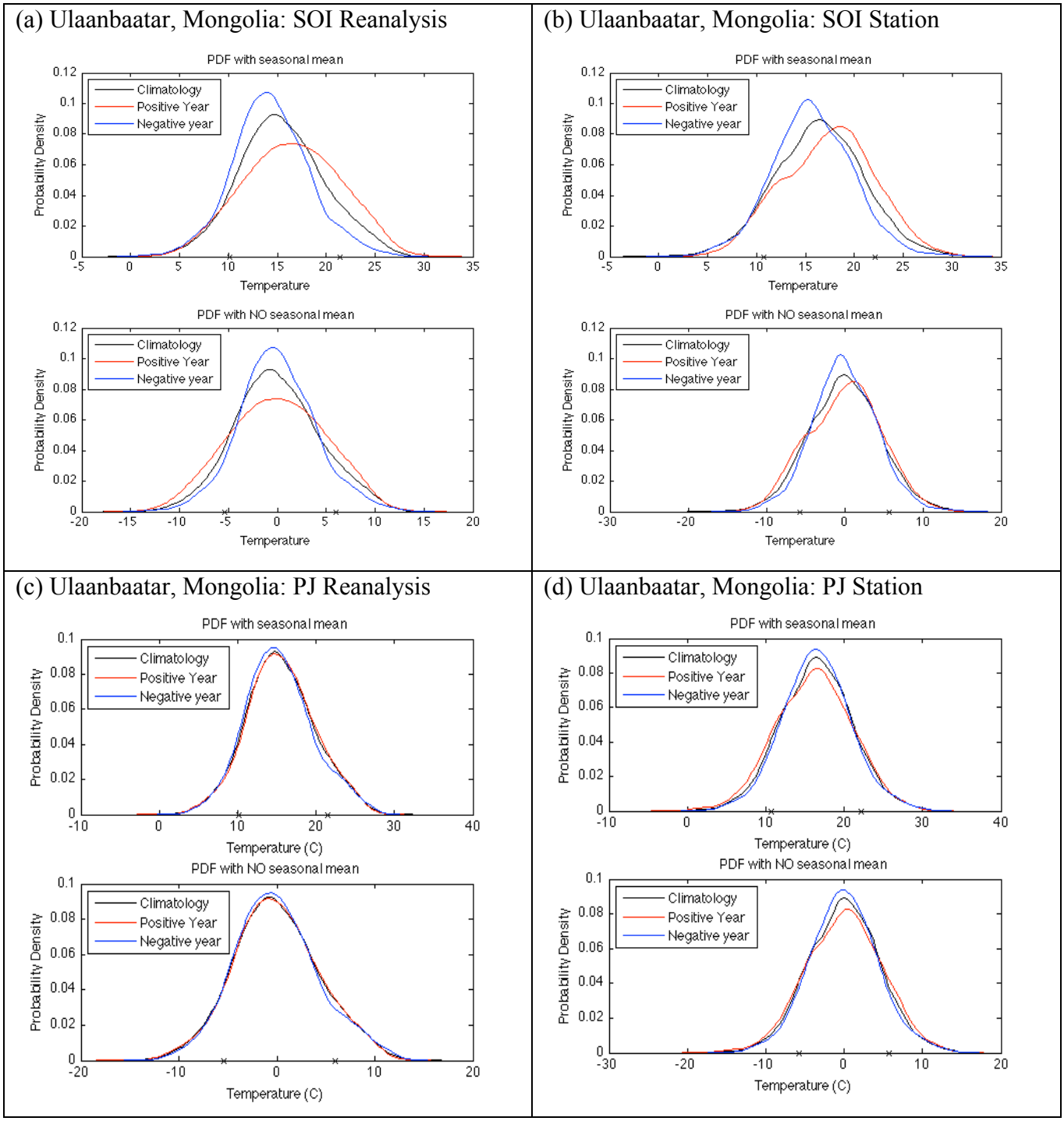

Figure 23
Smoothed histograms of daily mean SAT anomalies at Ulaanbaatar, Mongolia, based on phase of the SOI (a, b) and PJ (c, d), using the reanalysis data (a, c) and station data (b, d). Each composite consists of distribution in climatology (black), positive phase (red), and negative phase (blue). The upper plots in each figure are based on the raw anomalies and the lower plots are based on the anomalies with seasonal mean removed. The 10th and 90th percentiles of climatological PDF are shown as 'x' in each plot.

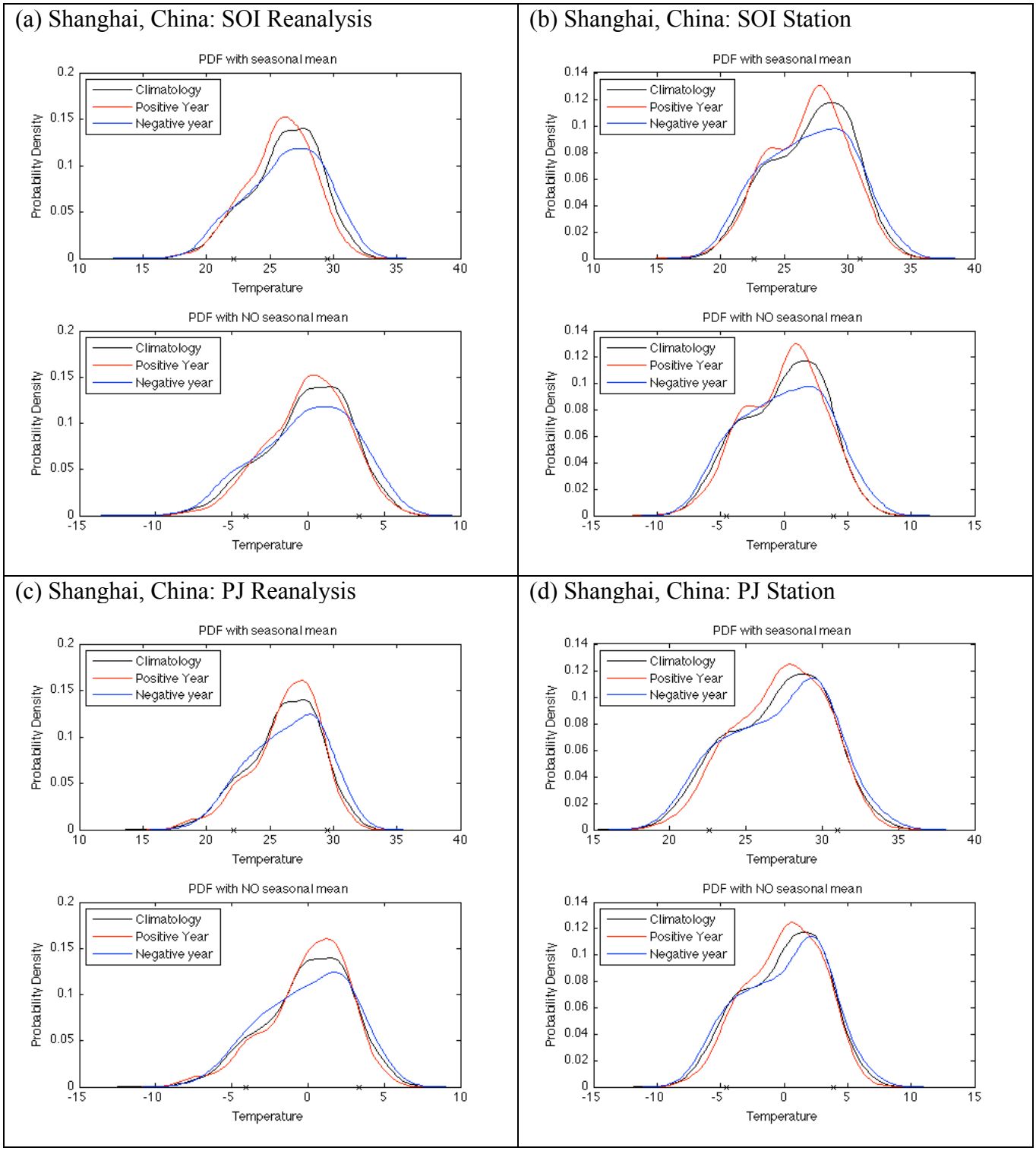

Figure 24
As in Fig. 23 but for Shanghai, China.